NTNU
Det skapande universitetet

Porøsitetstrender estimert fra sonic og seismiske p-bølge hastighetsdata.

Vegard Flatøy

Petroleumsfag
Innlevert: juni 2016
Hovedveiledar: Kenneth Duffaut, IPT

Noregs teknisk-naturvitskaplege universitet
Institutt for petroleumsteknologi og anvendt geofysikk

Problembeskrivelse

Utvikler model og metodikk for å estimere porøsitetstrender fra sonic og seismiske p-bølge hastighetsdata. Modellen er baser på en en konstruksjon av øvre og nedre grenser for elastisk moduli som en funksjon av leireinnhold og porøsitet.

Summary

We offer a new bounds based model and methodology to estimate low frequency porosity trends from velocity data with the opportunity to include lithological information via a clay content parameter, to improve estimations. Our approach is based on the construction of upper and lower bounds for the elastic moduli of an assumed binary lithology consisting of shale and sand with brine filled porosity. The upper and lower bounds are a functions of porosity and clay content and can for a given pair of velocity and clay content values yield porosity estimation and upper and lower porosity bounds. We apply our model on three data sets gathered at the Smørbukk, Sleipner and Snøhvit fields. Estimations of porosity are performed both without prior lithological information and with lithological information. A clear improvement of porosity estimations was found when including lithological information. Our proposed model and methodology is also applied to seismically derived velocities gathered at Snøhvit and Sleipner, yielding estimated porosity and estimated upper and lower porosity bounds for the entire 2D velocity sections.

Sammendrag

Vi utvikler med dette arbeidet en ny model og metodikk for å estimere lavfrekvente porøsitetstrender fra hastighets data med en mulighet for å forbedre estimert porøsitet ved å inkludere en litologisk parameter for leireinnhold. Vår fremgangsmåte er basert på konstruksjonen av øvre og nedre grenser for den elastiske modulus av en antatt binær litologi, bestående av skifer og sand med saltvann som porevæske. De øvre og nedre grensene er en funksjon av porøsitet og leireinnhold og vil for en gitt hastighet og et gitt leireinnhold kunne gi et estimat av porøsitet i tillegg til øvre og nedre grenser for porøsitet. Vi anvender modellen vår på tre datasett hentet fra Smørbukk, Sleipner og Snøhvit. Porøsitets-estimering blir utført både uten og med litologisk informasjon. Vi ser en klar forbedring i estimeringer av porøsitet når litologisk informasjon inkluderes. Vi anvender også modellen på seismiske hastigheter hentet fra Snøhvit og Sleipner som gir estimert porøsitet og øvre og nedre grenser for porøsitet for hele 2D seismiske hastighetsseksjoner.

Contents

1 Introduction

Porosity prediction based on velocity and especially sonic-log velocities has been subject to investigation ever since the beginning of oil exploration and production.

In both exploration and production of hydrocarbons it is essential to accurately determine geologic reservoir parameters such as porosity and permeability as these impact exploration and production potential in terms of value and efficiency. In order to achieve this, trying to link petrophysical properties with velocity has proven to be a cost effective but simultaneously challenging strategy.

Porosity is arguably one of the most difficult properties to estimate due to is complex nature and its non-unique relation to elastic rock properties. The elastic properties of rocks are a product of a wide range of factors such as mineralogy, burial history, pore-space topology, diagenesis, stress and many more, making it difficult to invert directly to porosity.

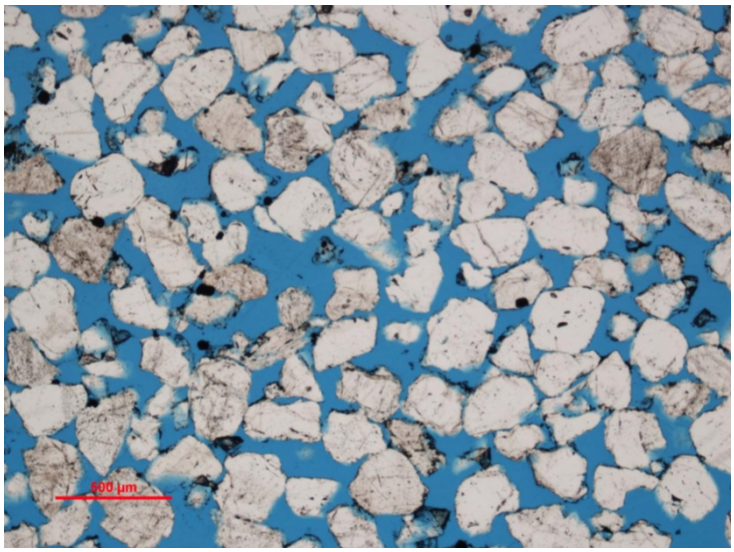

Figure 1: Thin-section illustrating the complex grain composition and geometries that make up porosity. This geometric complexity and the wide range of phenomena governing velocity; cementation, consolidation, pore pressure, makes it difficult to infer information on porosity from velocity alone. The depicted thin-section is a medium-grained quartz arenite from Fruholmen formation [Porten, 2012]. 2% quartz cement, 30% porosity.

Wave propagation in porous media has been described by many theoretical models [Gassman and Smit, 1951, Biot, 1956, Geertsma and Smit,

1961, Kuster and Toksöz, 1974]. Common for the theoretical models are their numerous assumptions, approximations and parameters incorporated to describe the elastic properties of a rock. This makes them poorly suited for prediction or inversion. In reality we have sparse data; seismic experiments offering an estimation of velocities or wells located often hundreds if not thousands of meters apart. With such small amounts and small variation of input data, the complexity of a theoretical model is rendered useless.

Empirical models, such as such as [Wyllie et al., 1956, Raymer et al., 1980, Tosaya and Nur, 1982, Kowallis et al., 1984, Han et al., 1986], offer another widely researched approach, based on simple empirical relations. Empirical models relate the elastic properties of a rock to porosity using fewer parameters than their theoretical counterpart. Empirical models in turn assume much more idealistic models than what is the rock-physical reality and are often dependent on local correctional factors or functions.

Regardless of the widespread use and research of the aforementioned relations, their inability to account for scattering in velocity-porosity data, especially in the unconsolidated domain, still makes them uncertain when used for predictive purposes.

There have been many contributions on estimating porosity based on seismic velocities in the literature. Such as geostatistical approach proposed by Doyen [1988] , Dvorkin and Nur [1996] using cementation theory, linear trends found by Vernik and Nur [1992], stochastic rock-physics modelling proposed by Bachrach [2006] and the method of Berryman et al. [2002], based on density and the Lame elastic parameter λ. The mentioned works are only a few out of many and meant to give you an impression of the wide variety of approaches taken to estimate porosity based on seismic velocity.

We introduce a new approach where our aim is to capture porosity trends based solely on velocity data. We justify our aim by emphasizing the fact that in seismic experiments, velocity is the main carrier of information and we argue that the advantage of simplicity when considering only velocity, outweighs potential ambiguities in the estimation. With regards to ambiguities we mitigate these by introducing an estimation of porosity bounds on top of the porosity estimation.

We assume a binary sand/shale-system in order to construct a velocity-porosity transform that provides us with an estimated porosity and a set of bounds for possible porosities. In our model we only require velocity data in order to carry out the estimation and an a priori lithological prediction in the form of a *clay content-parameter* to improve the accuracy of the estimation.

As mentioned the estimated bounds will handle ambiguity by functioning as a measure of uncertainty in our porosity estimation as well as give us information on the maximum and minimum possible porosities.

Our approach is based on the construction of upper and lower bounds for the elastic moduli of a binary lithology consisting only of shale and sand, with brine filled porosity. The upper and lower bounds are a function of porosity and clay content and can for a given pair of velocity and clay content values, yield upper and lower porosity bounds. We achieve this by modelling the elastic bounds of "pure sand" at the low end of the V_{cl}-domain and compressional velocity in shale at the high end of the V_{cl}-domain before we linearly interpolate between the two end-models.

From here, we will refer to our "pure sand"-model at the low end of the V_{cl}-domain as our "**Sand model**" and our model for compressional velocity in shale at the high end of the V_{cl}-domain as our "**Shale model**". We will proceed to describe the theoretical basis for our model, how we use it to construct our model and the methodology we use to apply it. We will test our model and methodology on different types of velocity data; wireline sonic logs and seismically derived velocity data from both imaging analysis and full waveform inversion.

2 Theory

In order to construct our model we need a solid theoretical foundation which is accordance with our assumptions of a binary system of shale and sand. In the following section we introduce a bounds model describing the elastic moduli of a composite material [Hashin and Shtrikman, 1963] which is the basis for the *sand model*. We present an elastic moduli to porosity model for shale [Vernik and Kachanov, 2010], based on a V_{cl} factor. Lastly we introduce you to an approach to estimating the expected elastic moduli within a set of bounds [Hill, 1952], which will be of use when deriving a porosity estimation from our bounds model.

2.1 Sand Model

For our sand model we have chosen the Hashin and Shtrikman [1963] bounds-model. It is based on the concept that in order to predict the elastic moduli of a porous rock you can obtain upper and lower bounds by only specifying the volume fraction and the elastic moduli of each of the phases.

Being the narrowest possible bounds this is seen as the best bounds model for an isotropic linear elastic rock, without specifying anything about pore or grain geometries[Mavko et al., 2009, chap 4].

Constant:	unit	Quartz	water
G	[GPa]	44.0	0
K	[GPa]	37.0	2.2
$M = K + \frac{4}{3}G$	[GPa]	95.7	2.2
ρ	[g/cm^3]	2.65	1.03

Figure 2: Table of elastic properties of quartz and water.

These bounds are seen as robust as they are free of assumptions and approximations and provide us with a valuable set of laws when studying mixed materials and interpolating their sorting and cementing trends as well as consistently describing suspensions and fluid mixtures which becomes important at critical porosity.

The Hashin-Shtrikman bounds for bulk and shear moduli respectively, for a mixture of two materials are defined as

$$K^{HS\pm} = K_1 + \frac{f_2}{(K_2 - K_1)^{-1} + f_1(K_1 + \frac{4}{3}G_1)^{-1}} \tag{1}$$

$$G^{HS\pm} = G_1 + \frac{f_2}{(G_2 - G_1)^{-1} + 2f_1(K_1 + 2G_1)/\Big(5G_1(K_1 + \frac{4}{3}G_1)\Big)^{-1}} \qquad (2)$$

where the subscripts 1 or two indicates if it is an elastic modulus of constituent 1 or 2. K indicate the bulk modulus, G is the shear modulus and f is the volumetric fraction of the given phase. Equation (1) and Equation (2) give upper bounds when the elastic moduli of the stiffest constituent is given subscript 1 and lower bounds when the softest constituent is given subscript 1.

As previously mentioned, in our model we assume a binary rock comprised of sand and shale, and in the sand-domain of our model we assume our system to only consist of quartz and brine. It is in this case we use Equation (1) and Equation (2) with quartz and brine as the two constituents. Their properties are given in Figure (2) and the resulting sand bounds are shown in Figure (3) and Figure (4).

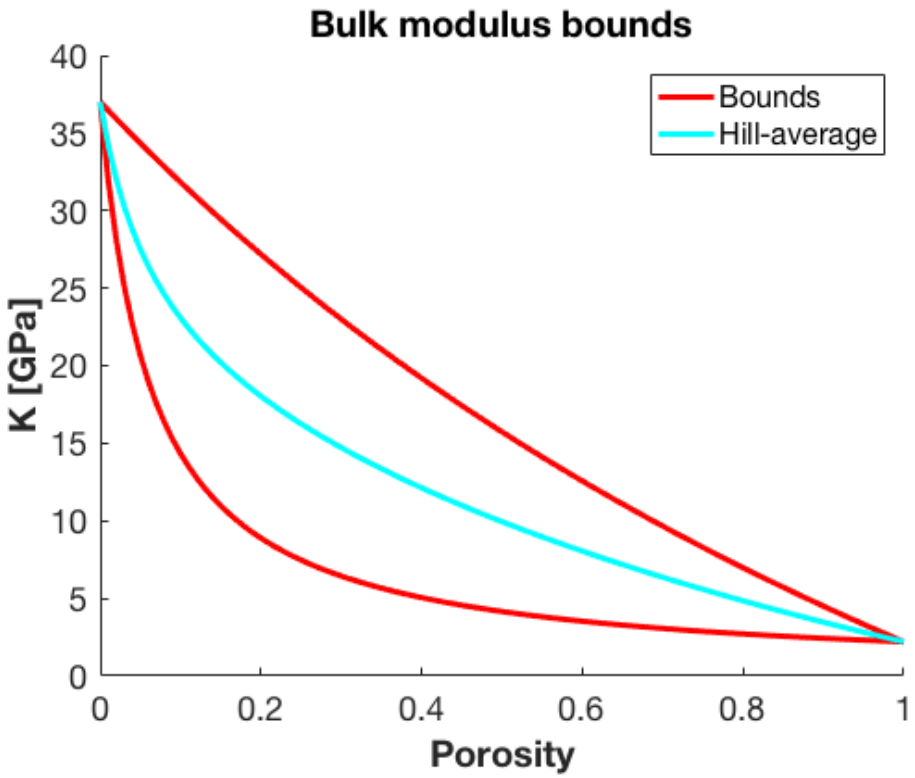

Figure 3: The red lines indicate the upper and lower bounds for the effective bulk modulus of a mixture of sand and brine, described by Equation (1). In this case the porosity will be the volumetric fraction of brine.

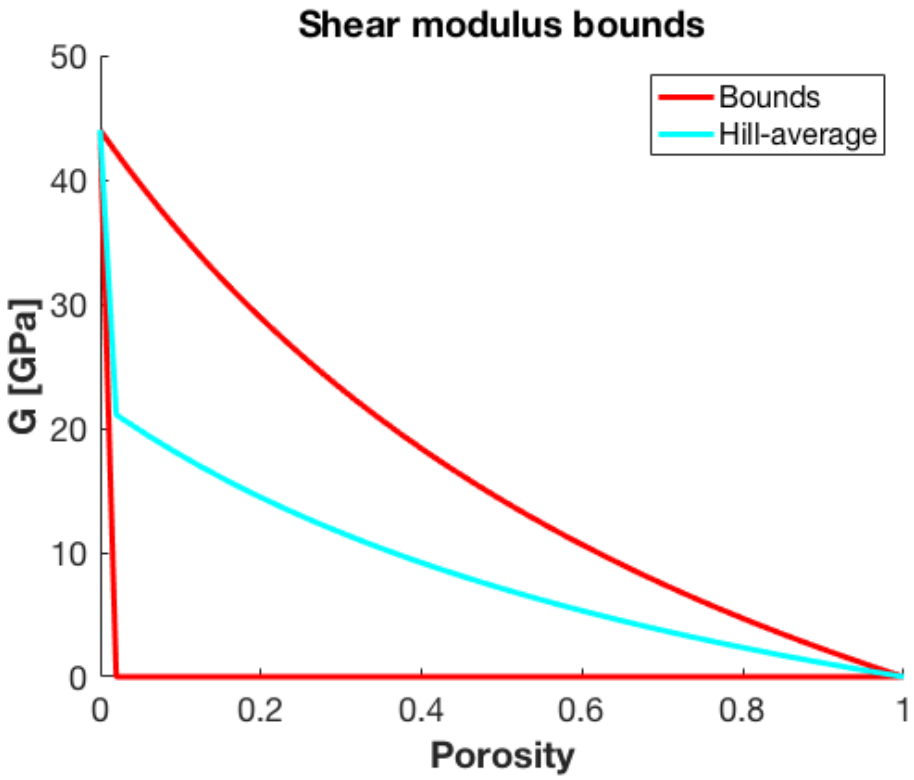

Figure 4: The red lines indicate the upper and lower bounds for the effective shear modulus of a mixture of sand and brine, described by equation (2). In this case the porosity will be the volumetric fraction of brine. Because the shear modulus of water is always zero we have to interpolate between zero and the upper bound in order for the velocity bounds in Figure (8) to meet at $\phi = 0$.

2.1.1 Validity and Assumptions

In this work we assume a fully brine saturated binary rock system composed of only sand and shale. Therefore in our sand model constructed by Hashin and Shtrikman [1963] bounds we only have two constituents, on our case quartz and water. The bounds described in Section (2.1) assume that both the rock and each constituent are isotropic and linear elastic.

2.2 Shale Model

After considering different models, the one proposed by Vernik and Kachanov [2010] proved to be most fitting as it relies on V_{cl} instead of focusing on shape factors, pore aspect ratio [Keys and Xu, 2002] and other parameters which are difficult to generalize and relate to velocities at seismic resolution.

Vernik and Kachanov [2010] created this empirical model based on two requirements which very much align with our own ambitions. (1) "based on first principles and contain only observable parameters such as porosity and clay content", (2) "should be immune from geographic peculiarities, i.e., applicable worldwide".

The anisotropic elastic constant for compressional wave velocity in the bedding normal direction is described by the following equations.

$$c_{33} = c_{33m}(1-\phi)^k \tag{3}$$

$$c_{33m} = \Big(\frac{V_{cl.ma}}{c_{33clay}} + \frac{1-V_{cl.ma}}{M_{qrtz}}\Big)^{-1} \tag{4}$$

$$k = 5.2 - 1.3V_{cl} \tag{5}$$

Where M_{qrtz} is the P-wave modulus of quartz, c_{33m} and c_{33clay} are the constants of the anisotropic solid matrix and its 100% clay equivalent respectively.

Note that we differentiate between $V_{cl.ma}$ in equation (4) and V_{cl} in (5), where $V_{cl.ma}$ is the ration of clay content in the matrix and V_{cl} is the ratio of clay content of the total rock volume. Both parameters are governed by the following equations

$$V_{cl} + V_{qz} + \phi = 1 \tag{6}$$

$$V_{cl.ma} + V_{qz.ma} = 1 \tag{7}$$

which lead to the relation

$$V_{cl} = V_{cl.ma}(1-\phi) \tag{8}$$

The resulting shale model is plotted in Figure (5).

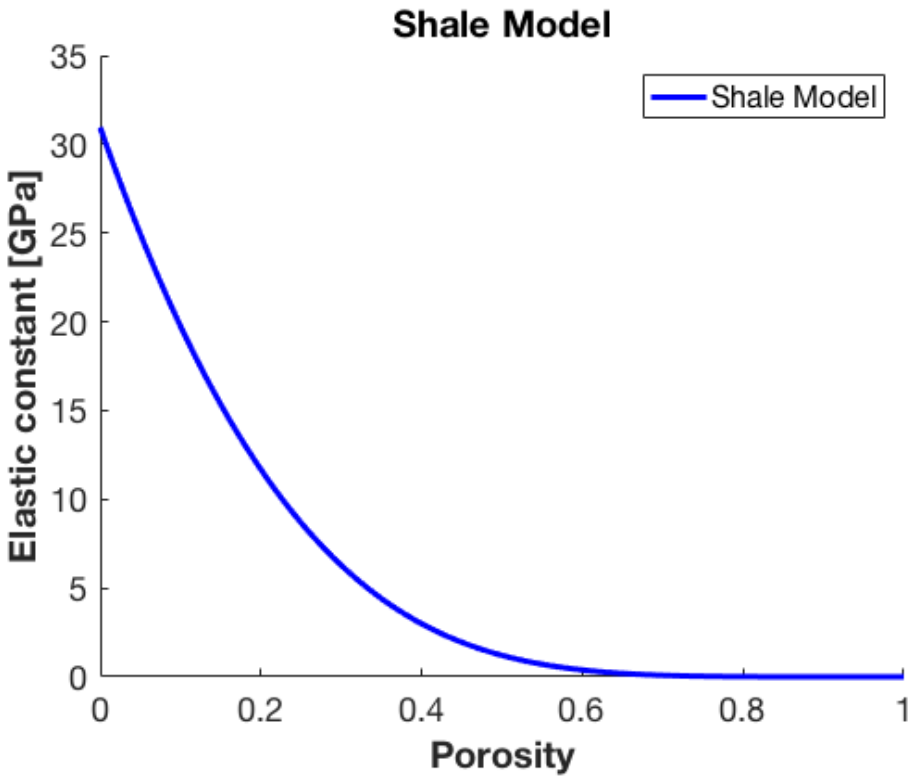

Figure 5: The anisotropic elastic constant for compressional wave velocity in the bedding normal direction, described by Equation (3)

2.2.1 Validity and Assumptions

As mentioned in Vernik and Kachanov [2010] this model limits itself to non-organic shales. Because non-organic shales have high capillary pressure they are nearly always fully water saturated and we avoid the need of fluid substitution.

In addition to this it is important to emphasize that this model is describes the elastic constant in beddingnormal direction.

As mentioned before we differentiate between V_{cl} and $V_{cl.ma}$, which is not the case in Vernik and Kachanov [2010]. In Figure (6) we find the difference between the equations in Vernik and Kachanov [2010] and what we argue to be a minimal improvement. The difference is not large but worth noting.

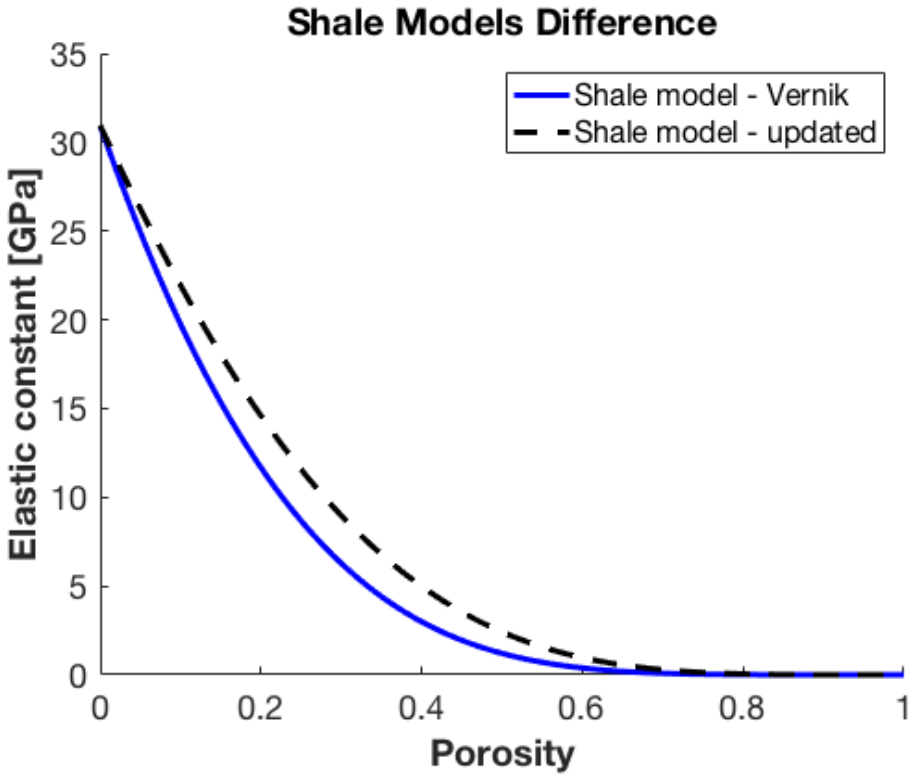

Figure 6: Difference between using $V_{cl.ma}$ vs V_{cl} in Equation (4). Black dashed line is using V_{cl}, the blue line is using $V_{cl.ma}$

2.3 Hill Average

Hill [1952] first introduced the the idea of estimating rock properties by averaging elastic bounds when they first proposed the average of the Voigt upper bound [Voigt, 1889] and the Reuss lower bound [Reuss, 1929], also known as *Voigt-Reuss-Hill average*. In this work we chose to use the arithmetic average of the Hashin-Shtrikman bounds as a means to estimate the expected porosity for a given velocity. We will simply call this the *Hill average*, described by Equation (9) [Mavko et al., 2009].

$$M_{Hill} = \frac{M_{HS^+} + M_{HS^-}}{2} \tag{9}$$

where M_{HS^+} and M_{HS^-} are respectively the upper and lower bound for the elastic moduli, derived from Equation (1) and Equation (2).

3 The Model

In order to predict porosity from velocity data we first transform our sand and shale models to the velocity domain using Equation (10) and Equation (11) respectively, where K and G are the bound models for bulk and shear moduli, described in Section (2.1). c33 is the shale model for elastic modulus, described in Section (2.2).

$$V_{sand} = \sqrt{\frac{K + \frac{4}{3} \cdot G}{(1-\phi)\rho_{qz} + \phi \cdot \rho_w}} \tag{10}$$

$$V_{shale} = \sqrt{\frac{c_{33}}{(1-\phi) \cdot \rho_{qz} + \phi \cdot \rho_w}} \tag{11}$$

Wireline sonic measurements have shown that in close to bedding normal direction velocities in non-organic shales show a stable and somewhat non-linear relation to porosity in the 0 - 40% porosity range[Vernik and Kachanov, 2010]. Above this porosity range the grains are usually no longer cemented in a matrix structure but rather loosely suspended in the pore fluid. In this regime we approximate the velocities in our shale model by assuming it cannot have velocities lower than water velocity, illustrated in Figure (8). We do not need the same constraint for our sand model as it is a product of water properties and we see the lower bound in Figure (8) approach water velocity as porosity increases.

In our work we assume a minimum quartz content of $V_{qz.ma} = 20\%$ regardless of porosity and clay content. This means a maximum clay content of $V_{cl.ma} = 80\%$ in Equation (4) when constructing our shale model. We argue that this assumption is reasonable in order to have our model correspond to reality where shales normally contain some amount of quartz and are rarely comprised of pure clay.

In order to further constrain our model to predict realistic porosities we take into account the maximum allowed physical porosity which occurs with cubic packing. The maximum possible porosity occurs when we have cubic packing of perfect spheres which gives a maximum porosity of $\phi = 0.476$ [Mavko et al., 2009, Table 5.1.1]. Grains are rarely spherical in reality which would cause us to believe that the maximum porosity is in fact lower than $\phi = 0.48$. Nevertheless we implement an upper porosity limit of $\phi = 0.48$ in our model to retain certainty that we in fact have a true upper limit for porosity. Sand and shale velocity models constrained by the mentioned assumptions are illustrated in Figure (8).

It is important to note that the Hill-average in Figure (8) is not the arithmetic average of the sand model velocity bounds. It is in fact the Hill-

average of the sand model elastic bounds from Figure (3) and Figure (4) converted to velocity using Equation (10).

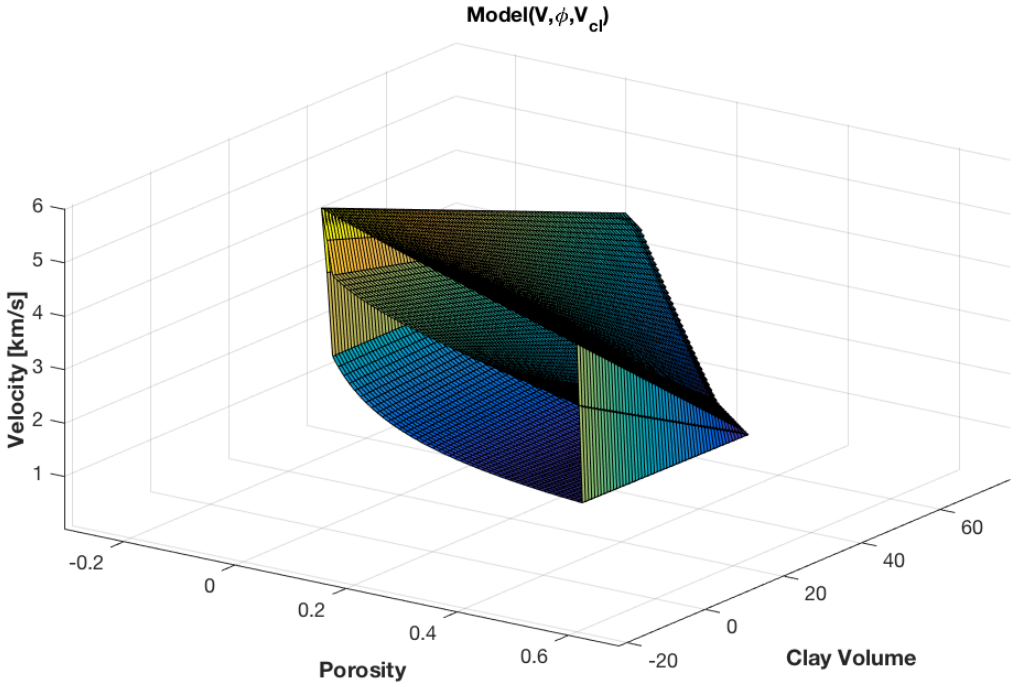

Figure 7: The model as a function of clay content, porosity and velocity. Along the "open end" of the model, where $V_{cl} = 0$, we have the **sand model** from Figure(8). Along the rear end of the model we have the shale velocity model also shown in Figure (8). In accordance to Equation (8), the **shale model** is implemented along $V_{cl.ma} = 80\%$[2] which corresponds to the diagonal in Figure (9). The three dimensional surfaces comprising the model are constructed by linearly interpolating from the sand models upper bound, lower bound and their Hill-average, to the shale model.

[2]80% because of our assumption of maximum 80% matrix clay content, described later in the text.

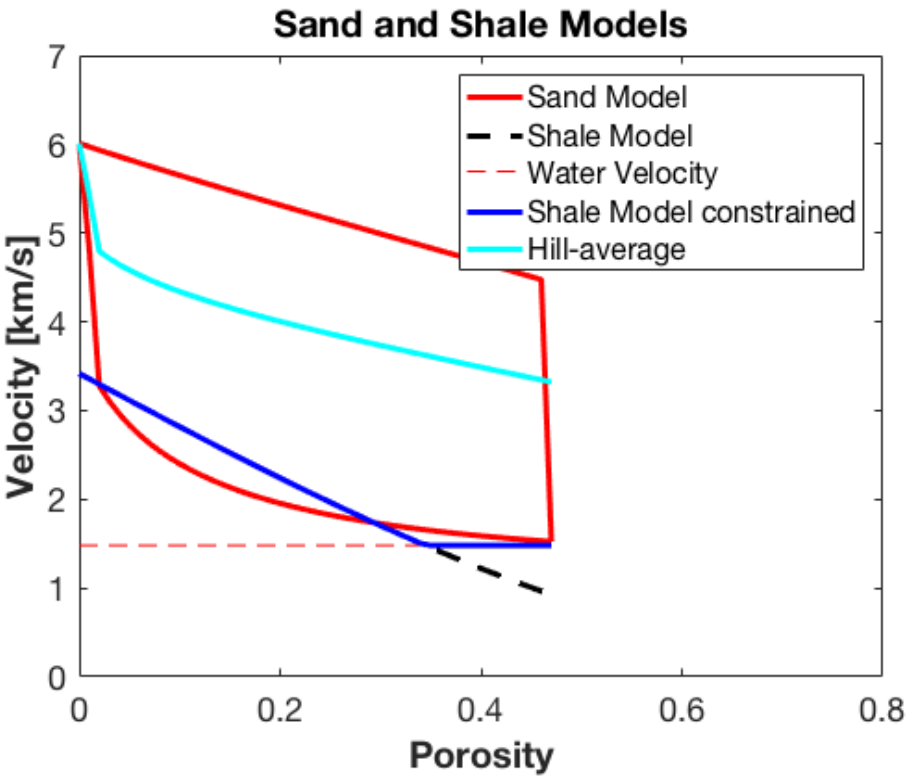

Figure 8: The red lines indicates the upper and lower velocity limits of our sand model where $V_{cl} = 0\%$. The dark blue line indicates the model shale model where $V_{cl.ma} = 80\%$. The dashed black line shows our shale velocity model if it did not adhere to water velocity in the unconsolidated regime. The cyan coloured line indicates the Hill-average of the bulk and shear limits converted to velocity using Equation (10). The Hill-average velocity lies closer to the upper limit because it is not an arithmetic average of the velocity limits but the Hill-average of the elastic bounds, converted to velocity.

When constructing our full three-dimensional model we implement our sand model along $V_{cl} = 0\%$ and our shale model along $V_{cl.ma} = 80\%$ (i.e the red sand bounds and the Hill-average in Figure (8) along the porosity axis in Figure (9) and the shale velocity model, blue line in Figure (8), along the diagonal in Figure (9)). In accordance with Equation (8) we implement our shale model along the diagonal because it is along this line we have a constant maximum clay content $V_{cl.ma} = 80\%$ and decreasing V_{cl} as porosity increases.

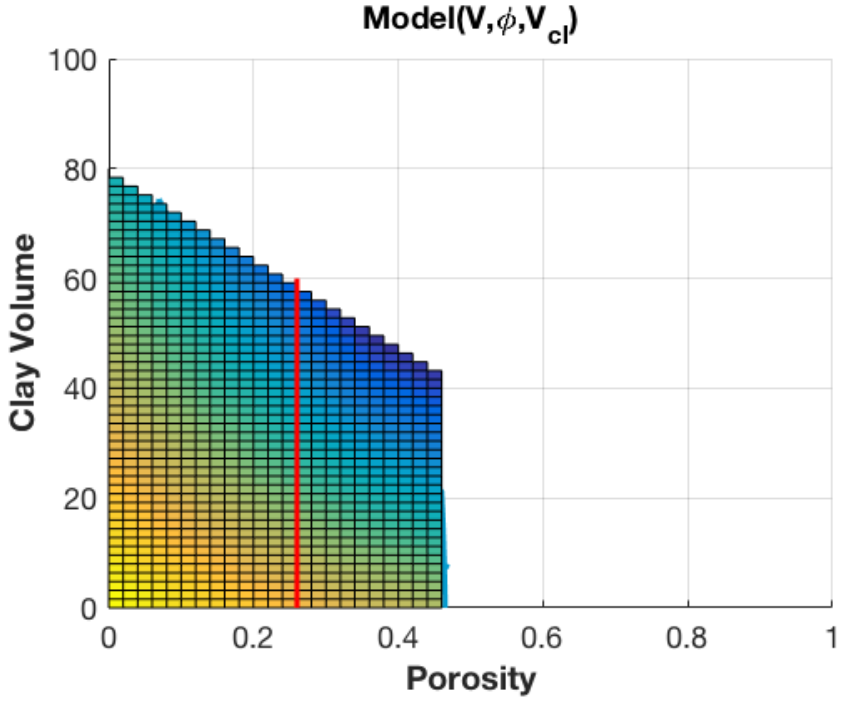

Figure 9: The model from Figure (7) seen in the (V_{cl}, ϕ)-plane (i.e Figure (7) seen from "above"). With our mentioned assumptions of a maximum porosity of 0.48 and a minimum quartz content of $V_{qz.ma} = 20\%$, we assume that there cannot exist (porosity, clay volume) -values outside the illustrated domain. The **red line** indicates the porosity along which we in Figure (10) illustrate our linear interpolation from sand model to shale model.

In order to construct the surfaces comprising our three-dimensional model, we perform a linear interpolation from the sand model placed along $V_{cl} = 0$, to shale model along $V_{cl.ma} = 80\%$. The interpolation is performed for each ϕ-value; from the upper bound, lower bound and Hill-average in our sand-model, to the corresponding ϕ-value of the shale velocity model, illustrated in Figure (10). This will result in the surfaces described and illustrated in Figure (7) at the beginning of this section.

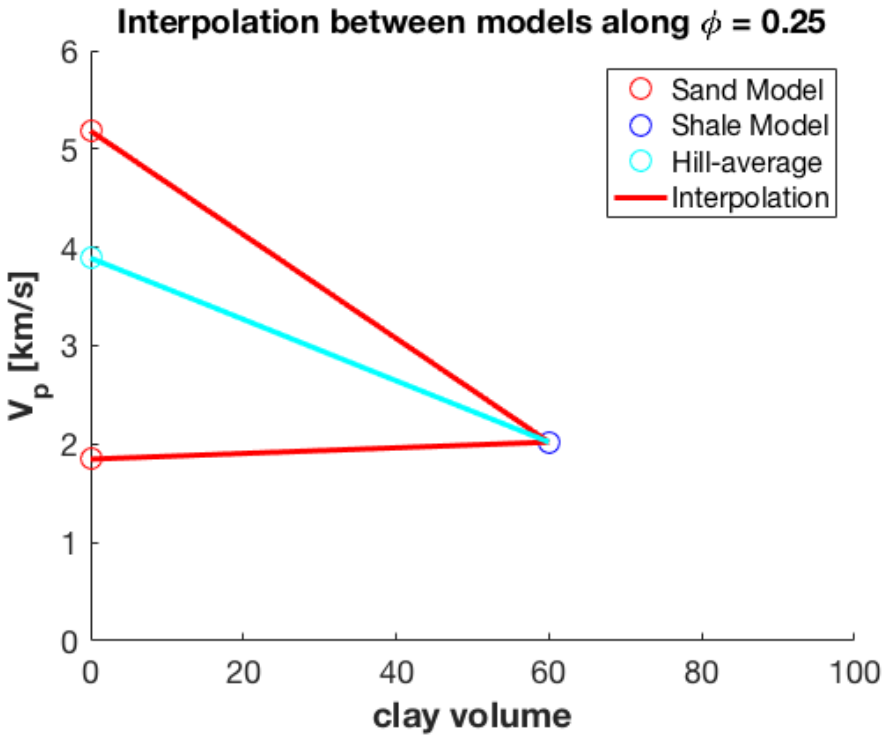

Figure 10: The linear interpolation performed to construct our three-dimensional model, shown for a cross section of our model along $\phi = 25\%$. We have three points located at; upper bound, lower bound and Hill-average in our sand model, at $\phi = 25\%$. From these three points we linearly interpolate to the one point located at $\phi = 25\%$ in our shale model.

In Figure (10) we see an example of how assuming $V_{cl.ma} = 80\%$ causes our shale model at $\phi = 25\%$ to be located at $V_{cl} = 60\%$. This fulfils Equation (8) where in this case we have $V_{cl} = 80\% \cdot (1 - 0.25) = 60\%$.

4 Methodology

When applying our model for porosity estimation we follow a simple two-step methodology for each velocity value. Whether it is a sonic-log, a 2D velocity section or a 3D velocity cube, the procedure is the same.

1. Insert velocity value in order to extract two dimensional "porosity-clay content"-model for the given velocity value.

2. Apply a priori lithological V_{cl} prediction to arrive at estimated porosity and porosity bounds.

4.1 Derive "porosity-clay content"-model for a given velocity value

With a velocity value obtained from any type of data, we derive a two-dimensional "porosity-clay content"-model which is valid for this particular velocity by finding the lines of intersection between a plane along the given velocity value and our model, illustrated in Figure (11).

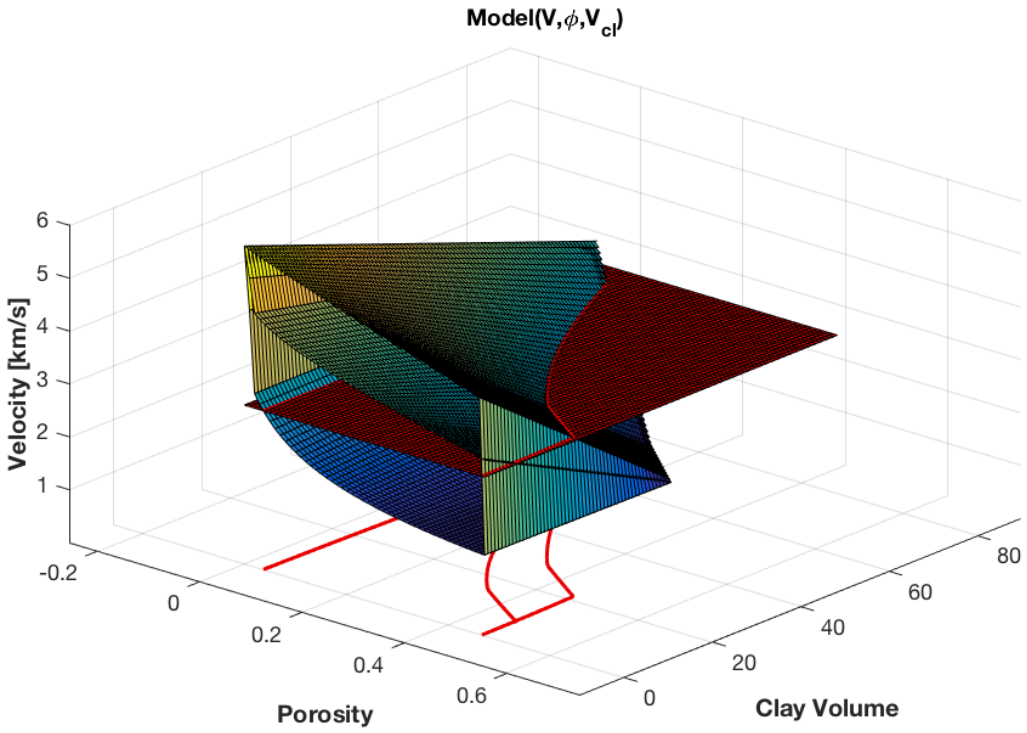

Figure 11: Our model plotted with an intersecting velocity plane, plotted in red along $V_{int} = 3km/s$. The lines of intersection can be seen projected onto the "Porosity-Clay Volume"-plane, where they form a new two-dimensional model for this exact velocity, also illustrated in Figure (12). Our new 2D-model can be seen as a limitation on all possible combinations of clay content and porosity that can produce a a given velocity value, in this case $V_{int} = 3km/s$.

We then proceed to project these lines of intersection onto the (porosity, clay content)-plane in order to arrive at our "porosity-clay content"-model which is valid for the given velocity value. An example is illustrated in Figure (12) for a velocity of 3 [km/s].

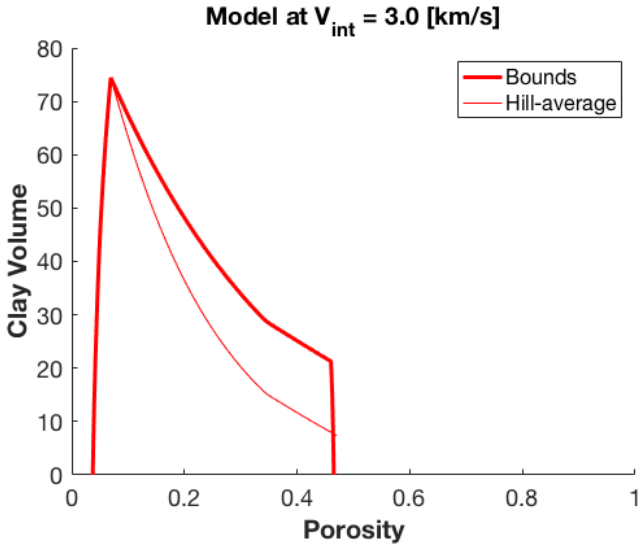

Figure 12: "porosity-clay content"-model for a velocity of 3 [km/s] obtained by projecting the lines of intersection between our three dimensional model and a plane along the given velocity, onto the (porosity, clay content)-plane. The thick red line to the right is from the intersection between the $V_{int} = 3km/s$-velocity plane and the upper bounds of our three-dimensional model, the thick red line to the left is from the intersection with the lower bound and the thin red line in the middle is from the intersection with the Hill-average-surface.

Our new two-dimensional model provides us with a set bounds for all possible combinations of clay content and porosity that can produce the given velocity. It is important to understand that we assume nothing about the clay and quartz content of the matrix as we only have knowledge of this at our end-models for sand and shale velocity. In our interpolation approach we only assume that the elastic behaviour of a composite system will trend linearly with increasing clay content, from a "pure sand" case to a "pure shale" case.

The intersection with the Hill-average surface, indicated by the thin red line in Figure (12), represents our estimation of the relation between clay content and porosity for a given velocity.

We can now easily imagine how keeping clay content constant and varying velocity would produce a variation of porosity estimations for a corresponding variation in velocity. This particular property is one of the major strengths of our model as this allows us to capture porosity trends with a simple lithological estimate of constant clay content. In other words; with nothing more than velocity data you are able to estimate porosity trends. In the case of improved lithological knowledge (e.g. V_{cl} estimate from GR-log or core samples) we are able to improve the estimation.

In Figure (12) we see that a decrease in clay content while velocity is kept constant will give an increased in porosity estimation. This is natural as clay has a lower compressional velocity than quartz and with decreasing clay content we have an increase in quartz content and thus porosity must increase in order to keep velocity constant.

4.2 Apply apriori lithological V_{cl} estimate

After having obtained a "porosity-clay content"-model for a given velocity, we apply an a priori lithological V_{cl}-prediction. By finding the intersection between a V_{cl}-prediction and our "porosity-clay content"-model we derive a porosity estimate and upper and lower porosity-bounds for the given velocity value.

The estimated porosity is derived from the intersection of our V_{cl} estimate and the middle line in Figure (13) which originates from the Hill-average of the upper and lower bounds.

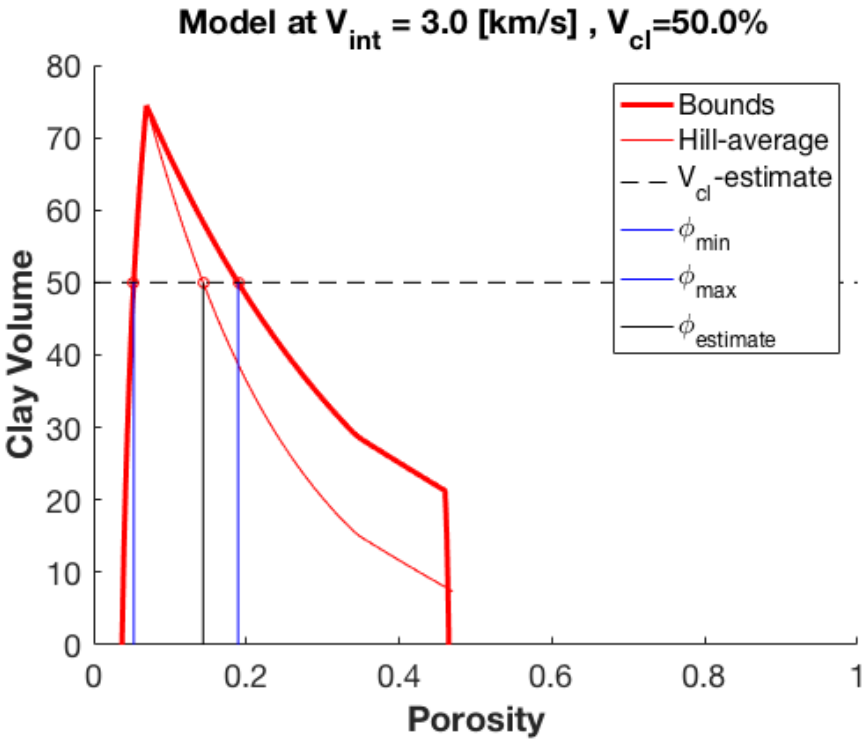

Figure 13: Our "porosity-clay content"-model for a given velocity of 3 [km/s]. With an a priori prediction of $V_{cl} = 50\%$ we derive the porosity bounds ϕ_{min}=0.0527 and ϕ_{max}=0.1892 and and and estimated porosity of $\phi_{estimated}$=0.1435 when $V_{int} = 3km/s$.

In order test our model and methodology we have obtained three different types of velocity data; velocity from sonic-log, seismically derived Normal-Moveout velocities and seismically derived velocities from full waveform inversion (FWI).

As our aim has been to construct a model with the ability to estimate low frequency porosity trends without any prior lithological information this will be the main focus when applying our model.

In the case of wireline sonic-log data we test our model using a simple guess of $V_{cl} = 50\%$, which corresponds to "no prior lithological information". From there we continue to asses the ability of our model to improve the estimation of the porosity trend when given additional lithological information. In all of the wells we have acquired data from we have also obtain gammray-log (GR) data, which will form the basis for our "additional lithological information".

We provide a V_{cl}-prediction based on the available GR-logs, using Equation (12) [Rider and Kennedy, 2011]. In order to predict clay content based on GR-log we first chose what we perceive to be the sand line, which corresponds to our choice for GR_{min}, and what we perceive to be the shale line, which corresponds to our choice of GR_{max}. A simplified illustration of this is shown in Figure (14).

$$V_{cl} = \frac{GR_{log} - GR_{min}}{GR_{max} - GR_{min}} \tag{12}$$

where GR_{log} is the value of the GR-log, GR_{min} is the picked value for the sand line and GR_{max} is the picked value for the shale line.

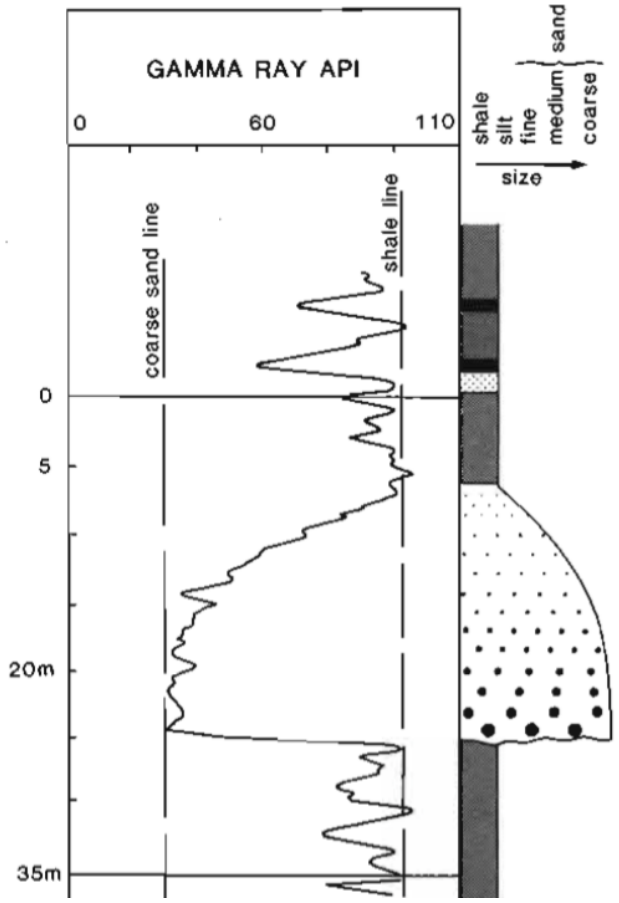

Figure 14: Gammaray-log[Rider and Kennedy, 2011] illustrating how we choose the **course sand line** and the **shale line**, corresponding to GR_{min} and GR_{max} respectively, when using Equation (12) to predict clay content. We see from Equation (12) that clay content will approach $V_{cl} = 0\%$ as GR_{log} approaches the sand line and $V_{cl} = 100\%$ as GR_{log} approaches the shale line. Lithologies corresponding to the different values of the GR-log is illustrated on the right.

For all the wells we have also gained access to density-log data. For comparative purposes we assume the porosity derived from the density-log to be true porosity.

Throughout our testing we plot porosity predicted from wireline density-logs alongside our estimation of porosity and its corresponding bounds. Porosity prediction based on density-log is derived from Equation (13)[Rider and Kennedy, 2011]. An example of this is illustrated in Figure (15) along with an example of clay content prediction based on GR-log.

$$\phi = \frac{\rho_{ma} - \rho_b}{\rho_{ma} - \rho_{fl}} \tag{13}$$

where ρ_{ma} is the matrix density, ρ_{fl} is the pore fluid density and ρ_b is the density value from the density-log. In our calculations we use $\rho_{ma} = 2.65$ [g/cm^3] and $\rho_{fl} = 1.03$ [g/cm^3].

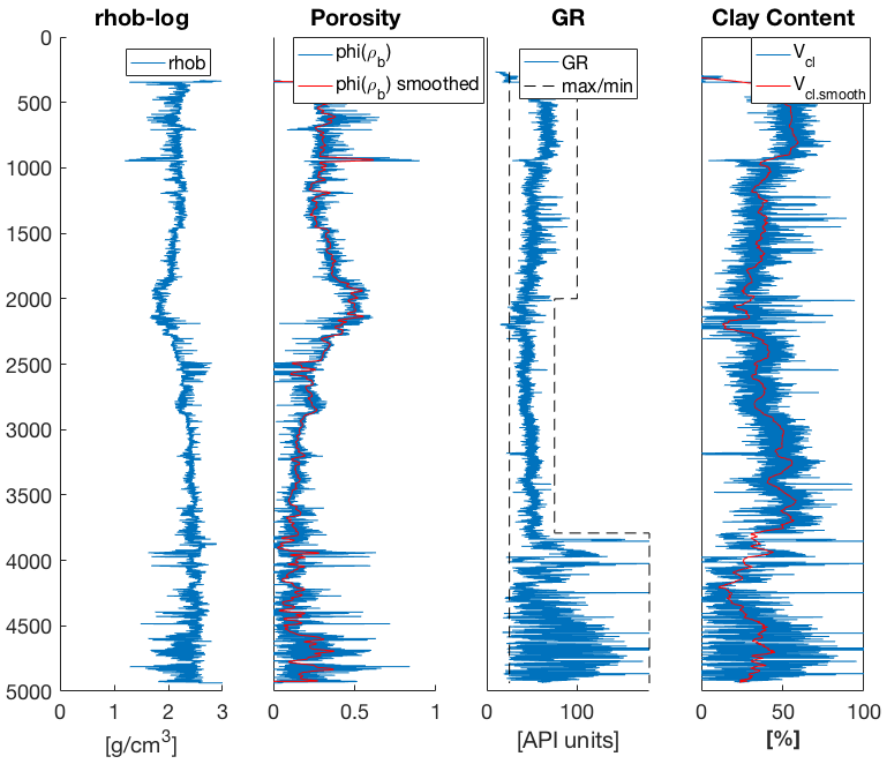

Figure 15: An example illustrating the prediction of porosity based on density-log values and the prediction of clay content based on GR-log values using Equation (13) and Equation (12), respectively. For this example Smørbukk well 6506/12-1 was used. Work on the same well is further illustrated in the Results section. Here we have used different GR_{max}/GR_{min} -values for different depth intervals. GR_{max}/GR_{min} values are listed in Figure (21).

5 Data Set

We test our model and methodology by applying it on data relating to three different locations on the Norwegian Continental Shelf, listed in Figure (5). From all of the three areas we have obtained wireline-data from in the form of sonic-logs and GR-logs, corresponding to the two types of data-input we utilize in our model; velocity and lithological data.

For each of the three areas we have also obtained density-log data. As mentioned at the end of Section (4.2) the density-log will we used to derive what we assume to be true porosity. We aim determine the quality of our own model's porosity estimation by comparing it to this density derived porosity.

Area	Field	Well	Seismically derived Velocity
Norwegian Sea	Smørbukk	6506/12-1	N/A
North Sea	Sleipner	15/9-13	FWI
Barents Sea	Snøhvit	7121/4-1	Normal-Moveout Velocity

Figure 16: Table showing the areas and corresponding fields and well number. The type of seismically derived velocity data for each area is listed to the right.

5.1 Norwegian Sea

From the Norwegian Sea area we have obtained data gathered at the the Smørbukk field. We have wireline velocity, density and gamma-ray data from well 6506/12-1. A comparative analysis of seismically derived data for this area is not available in this work.

5.2 North Sea

From the North Sea area we have obtained data gathered at the Sleipner field. We have wireline velocity, density and gamma-ray data from well 15/9-13. We have also obtain a three-dimensional velocity cube derived from from Full Waveform Inversion (FWI), covering an area containing well 15/9-13.

nx:	220	dx:	12.5m
ny:	660	dy:	12.5m
nz:	229	dz:	6.25m

Figure 17: Number of samples in Sleipner FWI velocity-cube and its spatial sampling.

Well 15/9-13 is located inside the FWI cube at UTM location:

UTM-x	437653.70
UTM-y	6470978.02

Figure 18: UTM location of well: 15/9-13

The FWI velocity cube was provided by Børge Arntsen. Further research and the work behind it can be read in Raknes et al. [2015].

5.3 Barents Sea

From the Barents Sea area we have obtained data gathered at the Snøhvit field. We have wireline velocity, density and gamma-ray data from well 7121/4-1 and a 2D interval velocity section intersecting the well location. The 2D interval velocity section is derived from Normal-Moveout velocity analysis [Dix, 1955]. The 2D section velocity data is given as a function of travelime. In order to relate the seismic data to well data we chose to convert travel-time data to depth using Equation (14).

$$z_i = \sum_{i=1}^{n} \frac{\Delta t_i V_{P.int_i}}{2} \tag{14}$$

nx:	178	dx:	
nt:	96	dt:	0.05s

Figure 19: Number of samples in Snøhvit 2D interval velocity section and its spatial and time sampling.

6 Results

We have estimated the porosity and its bounds by applying our model and methodology. For all of the data sets relating to the fields listed in Section (5). We wish to investigate our model's ability to estimate the low frequency porosity trend with solely velocity as input. We do this by applying a simple assumption of constant clay content where $V_{cl} = 50\%$ for all depths.

Further we asses the improvement of our model's estimation by including improved lithological information in the form of a clay content curve based on the GR-log as described at the end of Section (4.2).

6.1 The Smørbukk Field, Well 6506/12-1

6.1.1 Constant $V_{cl} = 50\%$

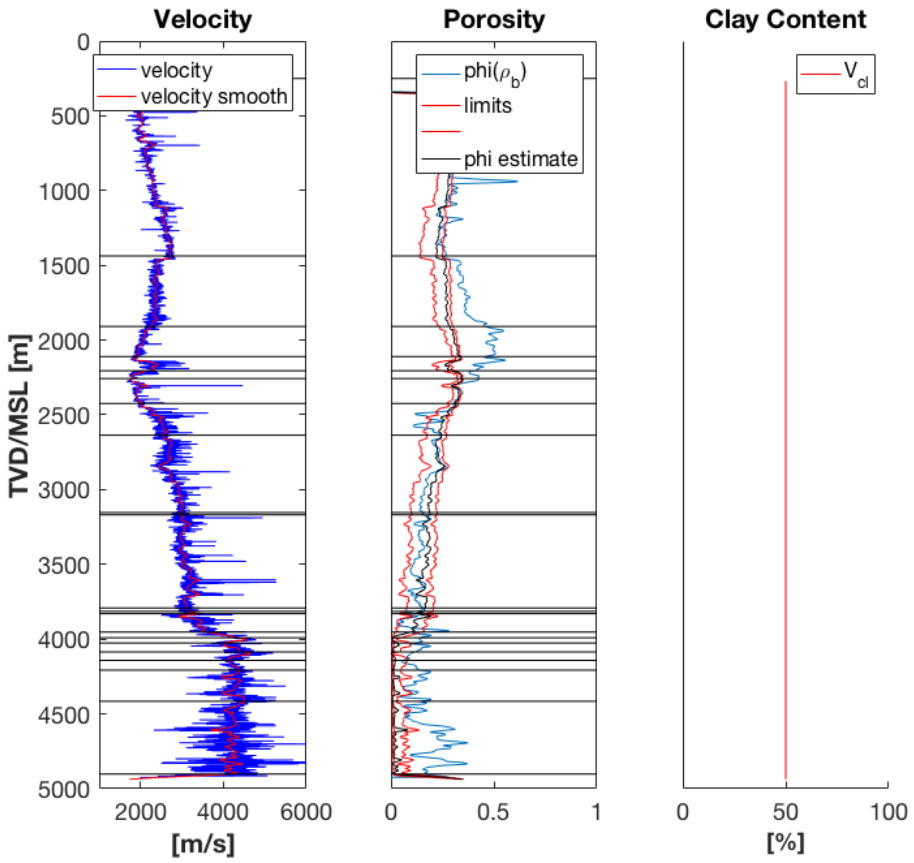

Figure 20: Left: V_p-log derived from the sonic-log. Middle: Red curves are estimated upper and lower porosity bounds along with estimated porosity in black, using our model. The blue curve is porosity estimated from the density-log as described in Section (4.2). Right: Curve indicating our assumption of constant clay content for all depths. Zero depth represents mean sea level.

6.1.2 Variable Clay Content

Depth interval	GR max	GR min
0 - 2000m	25	100
2000m - 3800m	25	75
3800m - 5000m	25	180

Figure 21: Table showing GR_{min} and GR_{max} values to predict V_{cl} in Smørbukk well 6506/12-1

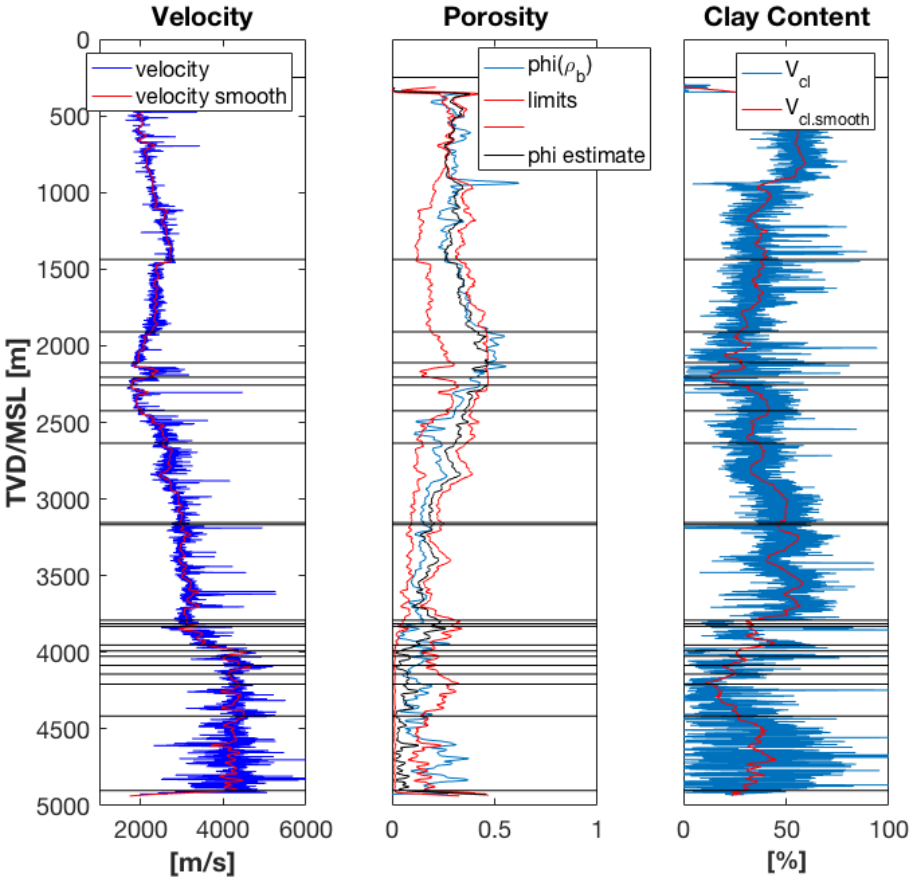

Figure 22: Left: V_p-log derived from sonic-log. Middle: Red curves are estimated upper and lower porosity bounds along with estimated porosity in black, using our model. The blue curve is porosity estimated from the density-log as described in Section (4.2). Right: Clay content curve estimated from GR-log, also described in Section (4.2). Zero depth represents mean sea level.

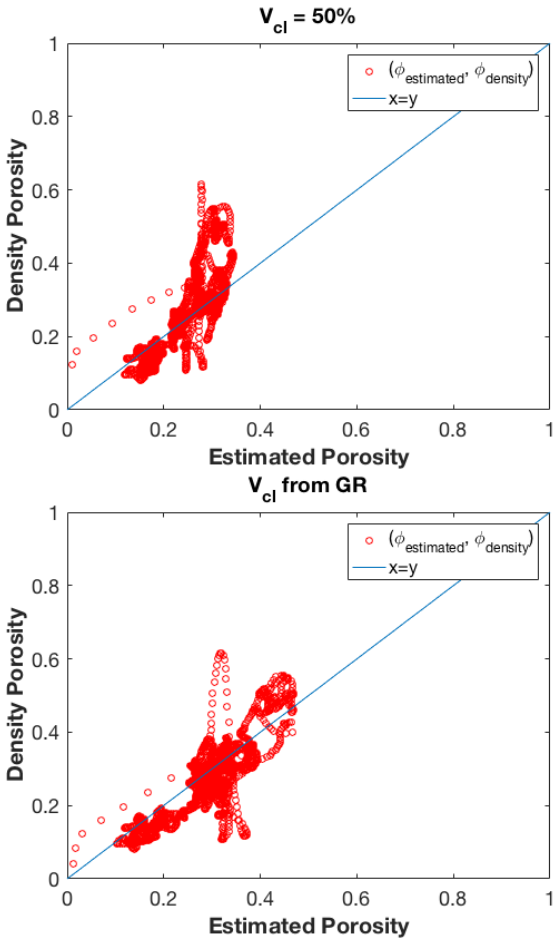

Figure 23: Estimated porosity values plotted against porosity predicted from density-log. Top: Porosity values estimated by our model with an simple prediction of constant $V_{cl} = 50\%$ (black curve in Figure (20)). Bottom: Porosity values estimated using our model with V_{cl} prediction based on GR-log (black curve in Figure (22)).

6.2 The Sleipner Field, Well 15/9-13

6.2.1 Constant $V_{cl} = 50\%$

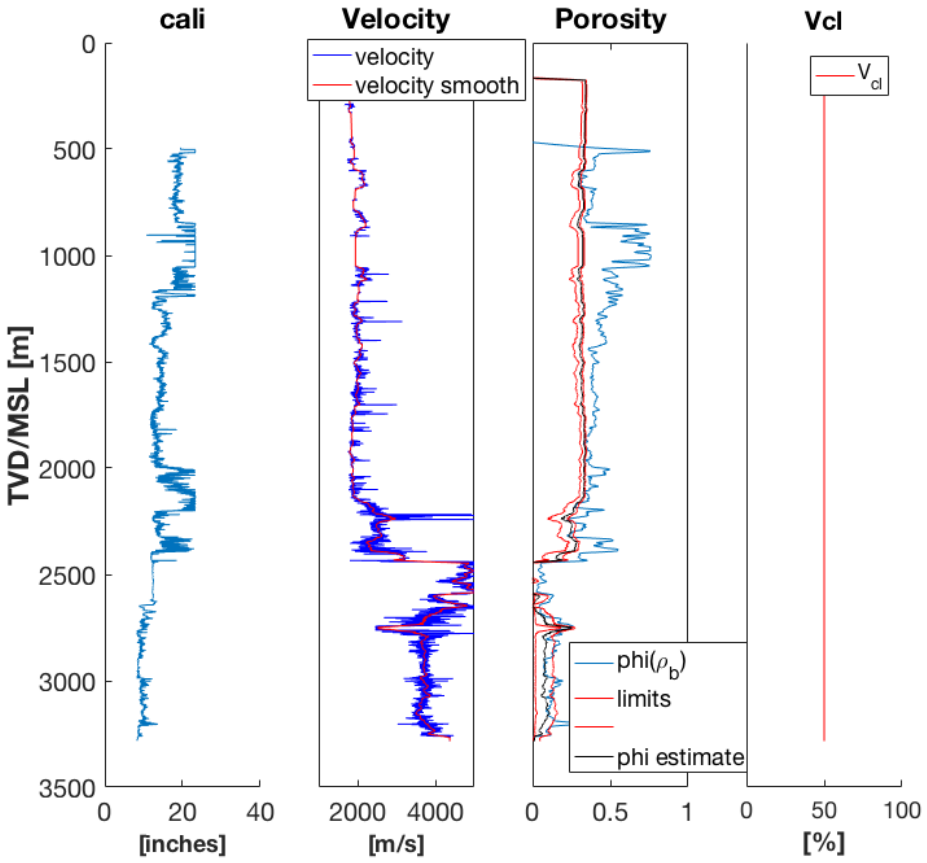

Figure 24: First: Caliper-log where we see indications of caving at multiple depth sections. Second: V_p velocity from sonic log. Third: Red curves are estimated upper and lower porosity bounds along with estimated porosity in black, derived from our model and method. The blue curve is porosity predicted from density-log described in Section (4.2). Fourth: Clay content curve indicating our assumption of constant clay content for all depths. Zero depth represents mean sea level.

6.2.2 Variable Clay Content

Depth interval	GR max	GR min
entire depth	10	170

Figure 25: Table showing GR_{min} and GR_{max} values to predict V_{cl} in Sleipner well 15/9-13.

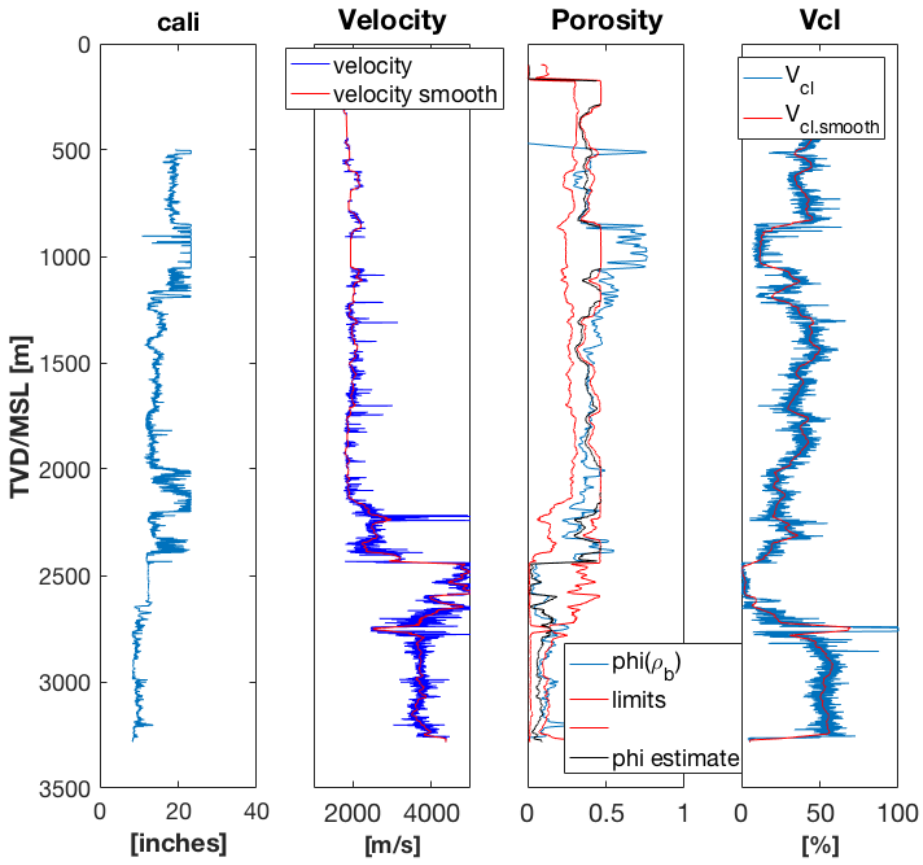

Figure 26: First: Caliper-log where we see indications of caving at multiple depth sections. Second: V_p velocity from sonic log. Third: Red curves are estimated upper and lower porosity bounds along with estimated porosity in black, derived from our model and method. The blue curve is porosity predicted from density-log described in Section (4.2). Fourth: Clay content curve predicted from GR-log also described in Section (4.2). Zero depth represents mean sea level.

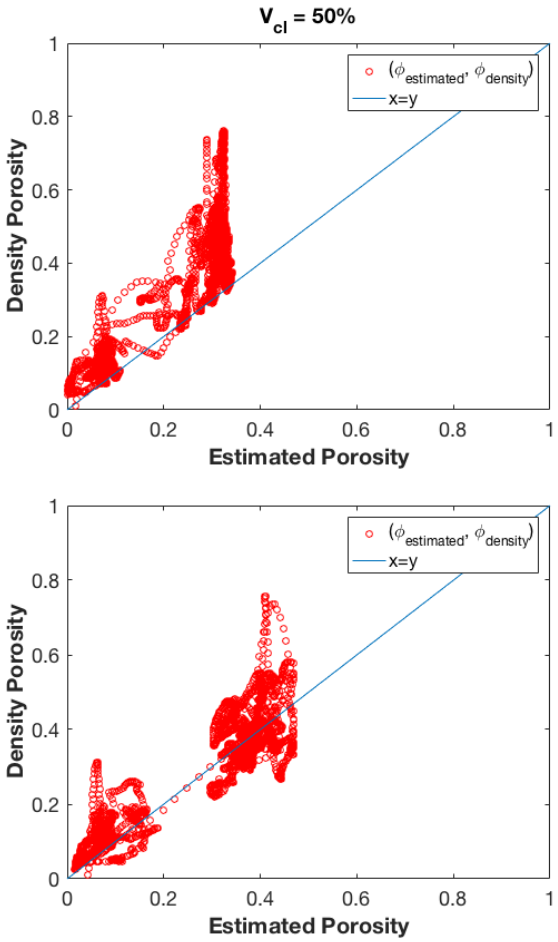

Figure 27: Estimated porosity values plotted against porosity predicted from density-log. Top: Porosity values estimated by our model with an simple prediction of constant $V_{cl} = 50\%$ (black curve in Figure (24)). Bottom: Porosity values estimated using our model with V_{cl} prediction based on GR-log (black curve in Figure (26)).

6.2.3 Profile from Velocity Cube

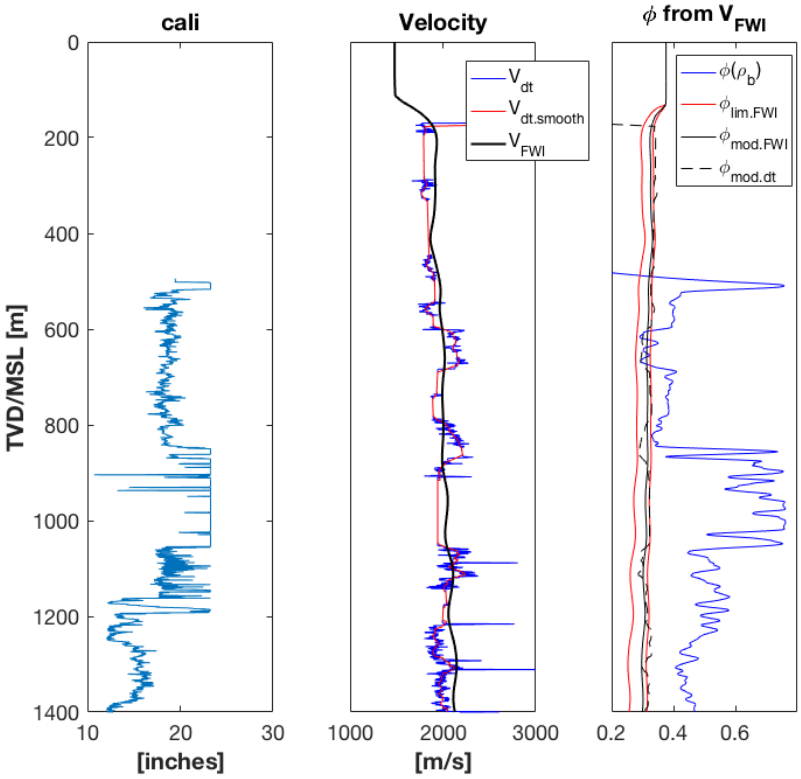

Figure 28: Left: Caliper-log where we see indications of caving. Middle: V_p velocity from sonic log along with 1D velocity profile plotted in black, extracted from 2D FWI velocity section in Figure (29), at well location. Right: Red curves are estimated upper and lower porosity bounds based on 1D velocity profile from 2D velocity section, along with estimated porosity in black, derived from our method. The blue curve is porosity predicted from density-log using Equation (13), described in Section (4.2). The black dashed curve is porosity estimated using our method on the sonic log (i.e. the black curve in Figure (24)). Estimations based on constant V_{cl}=50%.

6.2.4 2D Porosity Profiles

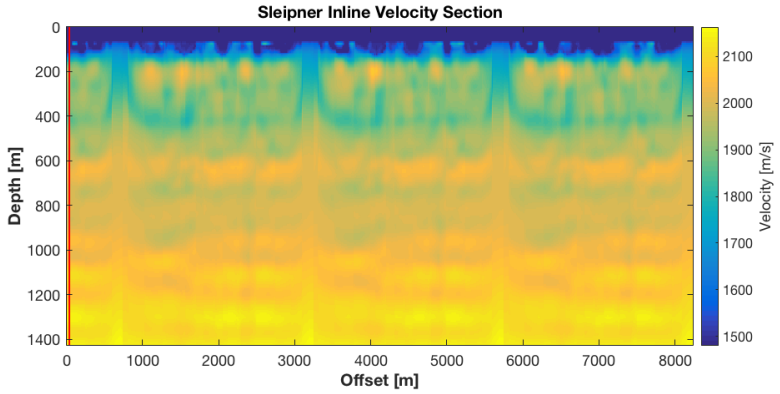

Figure 29: Inline 2D interval velocity section, crossing well (15/9-13), marked by the red line. Obtained from Full Waveform Analysis done by Raknes et al. [2015].

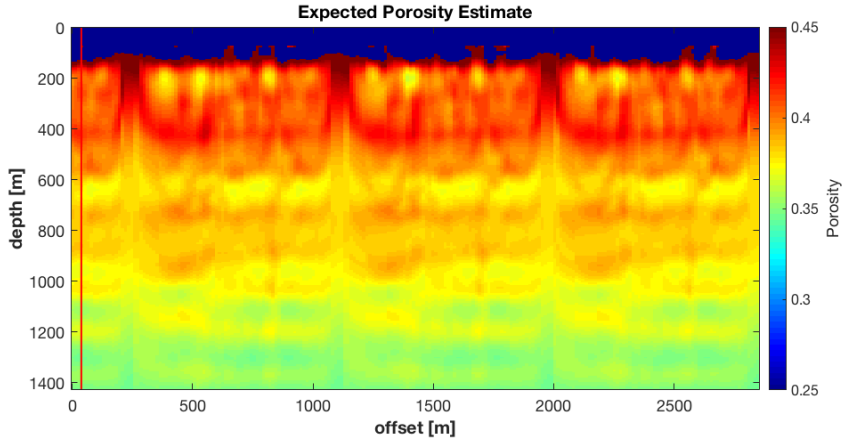

Figure 30: Estimated porosity calculated for the entire 2D-section in Figure (29). This corresponds to the estimated porosity in Figure (24). Estimations based on constant V_{cl}=50%.

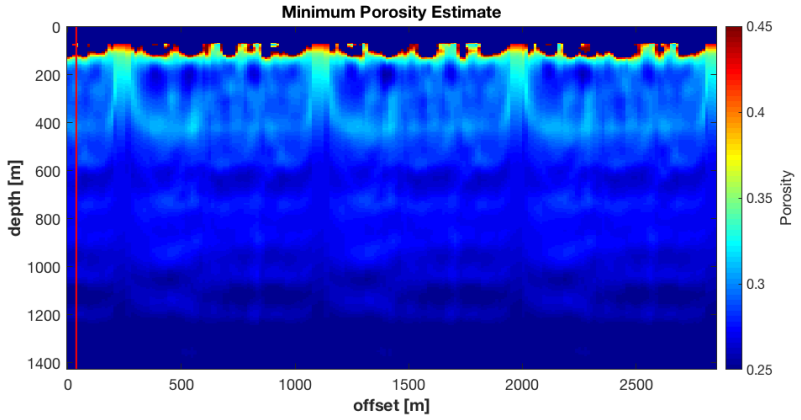

Figure 31: Lower porosity bound calculated for the entire 2D-section in Figure (29). This corresponds to the lower porosity bound in Figure (24). Estimations based on constant V_{cl}=50%.

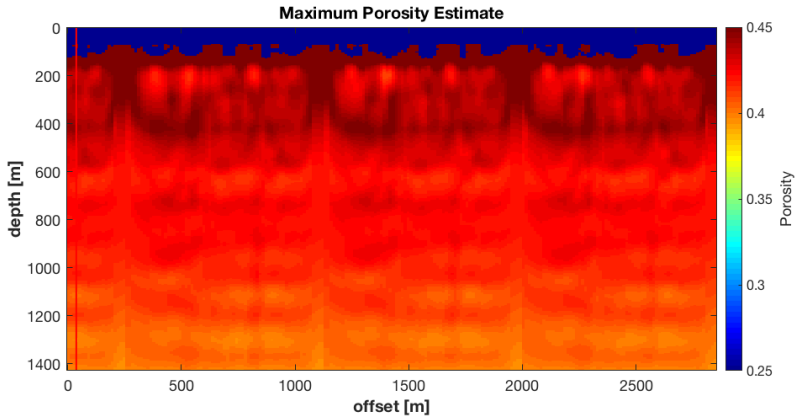

Figure 32: Upper porosity bound calculated for the entire 2D-section in Figure (29). This corresponds to the upper porosity bound in Figure (24). Estimations based on constant V_{cl}=50%.

2D porosity sections in Figures (30-32) are plotted for the same range of porosity values in order to compare the three resulting sections.

6.3 The Snøhvit Field, Well 7121/4-1

Checkshot data from well 7121/4-1 indicates slightly too high sonic-log velocities and too low seismic velocities.

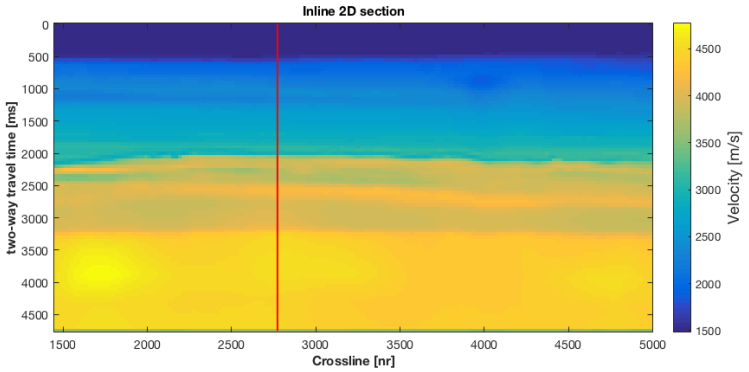

Figure 33: Inline 2D velocity section crossing well 7121/4-1 marked by the red line. Obtained from normal-moveout velocity analysis using Dix [1955].

In order to correct the well log velocities we integrate the log using Equation (15) to arrive at synthetic travel time values. We perform a simple correction by scaling the V_p-log by a factor of 0.975 in order to fit the travel time versus depth values from the sonic-log to the checkshot values, illustrated in Figure (34).

$$t_n = \sum_{i=1}^{n} \Delta t_i = \sum_{i=1}^{n} \frac{2\Delta z_i}{V_{p.int_i}} \tag{15}$$

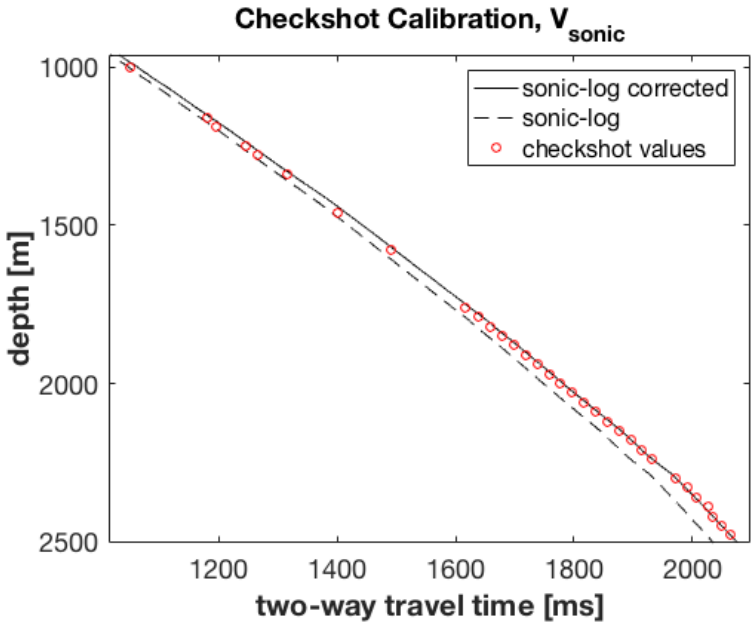

Figure 34: Checkshot values marked in red. The dashed curve is depth versus travel time values derived by integrating interval velocities from sonic-log using Equation (15). The dashed curve indicates slightly too high velocities from sonic-log, which caused us to perform a simple checkshot calibration by scaling the V_p-log by a factor of 0.975, arriving at the black curve which aligns with the checkshot values.

6.3.1 Constant $V_{cl} = 50\%$

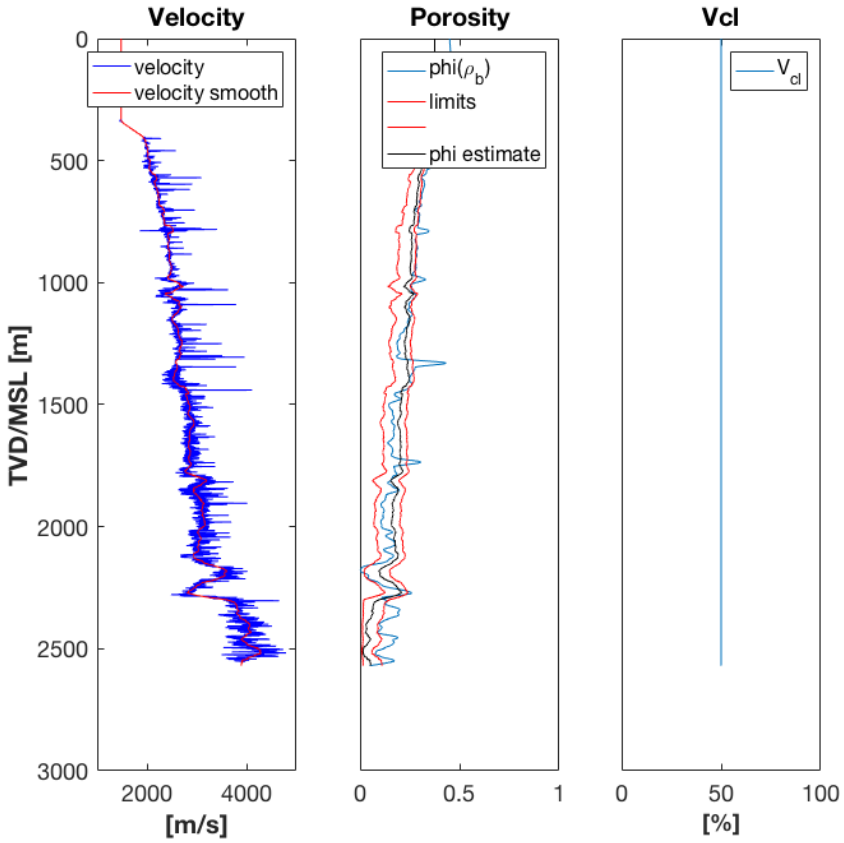

Figure 35: Left: V_p velocity from sonic log. Middle: Red curves are estimated upper and lower porosity bounds along with estimated porosity in black, derived using our model. The blue curve is porosity predicted from the density-log using Equation (13) described in Section (4.2). Right: Clay content curve illustrating our assumption of constant clay content for all depths. Zero depth represents mean sea level.

6.3.2 Variable Clay Content

Depth interval	GR max	GR min
entire depth	7	125

Figure 36: Table showing GR_{min} and GR_{max} values to predict V_{cl} in Snøhvit well 7121/4-1.

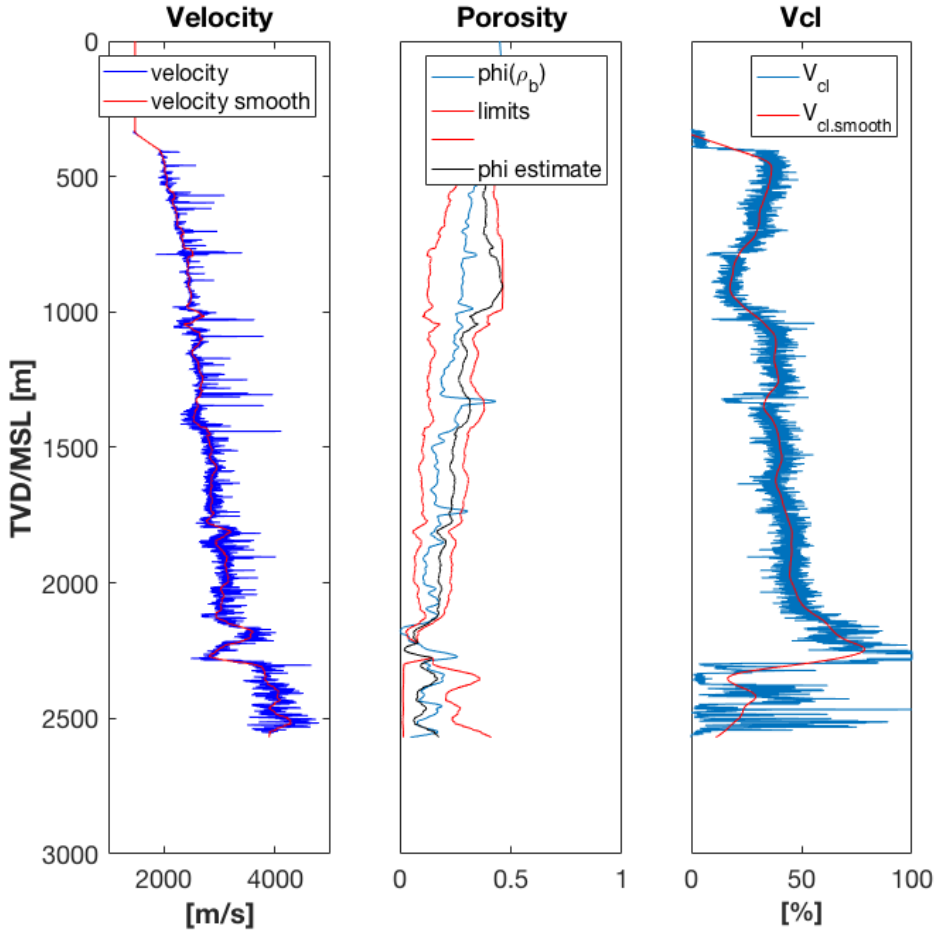

Figure 37: Left: V_p velocity from sonic log. Middle: Red curves are estimated upper and lower porosity bounds along with estimated porosity in black, derived using our model. The blue curve is porosity predicted from the density-log using Equation (13) described in Section (4.2). Right: Clay content curve predicted from GR-log also described in Section (4.2). Zero depth represents mean sea level.

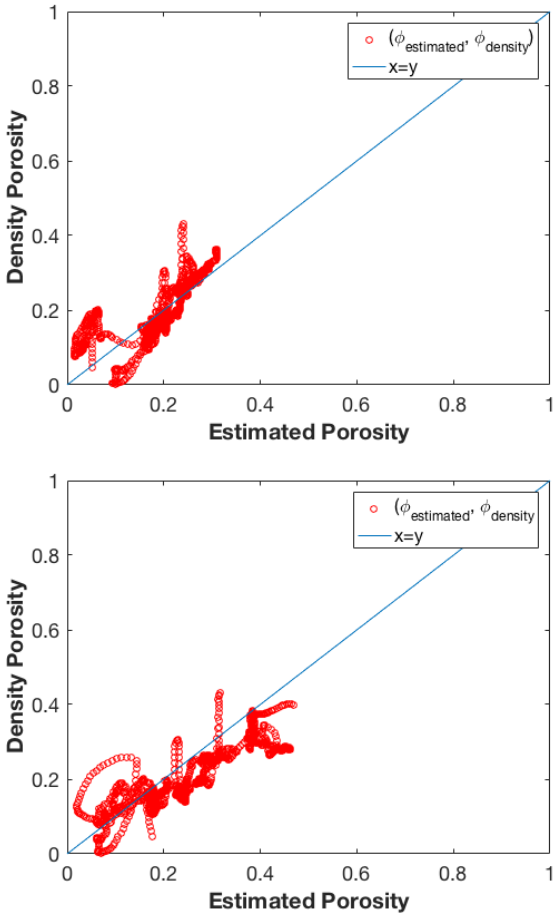

Figure 38: Estimated porosity values plotted against porosity predicted from density-log. Top: Porosity values estimated by our model with an simple prediction of constant $V_{cl} = 50\%$ (black curve in Figure (35)). Bottom: Porosity values estimated using our model with V_{cl} prediction based on GR-log (black curve in Figure (37)).

6.3.3 Profile from Velocity Cube

In order to correct the interval seismic velocities extracted along a line in a 3D velocity volume, we use Equation (16) with $\delta = -0.028$ which provides us with a reasonable fit to the the travel time versus depth values from the checkshot, illustrated in Figure (34).

$$V_{P0_i} = \frac{V_{P.NMO_i}}{(1-2\delta)^{\frac{1}{2}}} \tag{16}$$

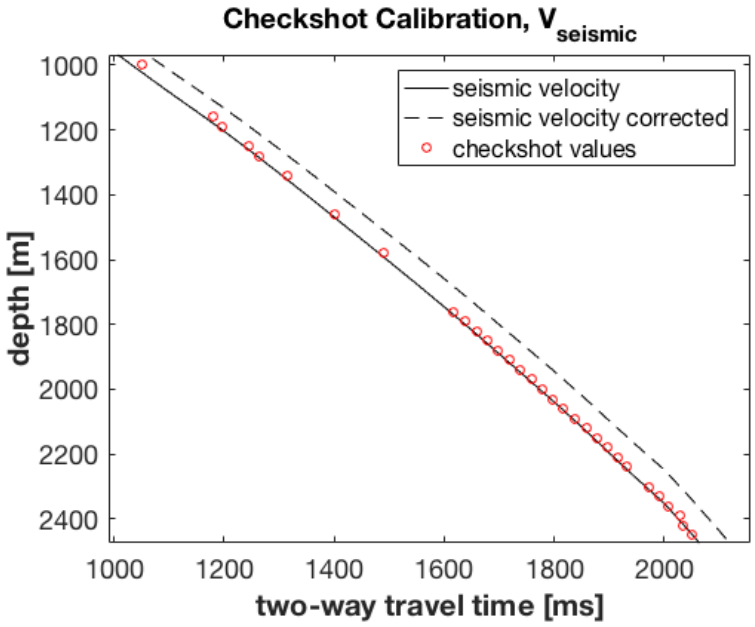

Figure 39: Checkshot values marked in red. The dashed curve is travel time values versus depth for the interval velocities extracted from the 2D NMO velocity section, at well location. The dashed curves indicates slightly too low velocities from in the NMO velocity secion, which caused us to perform a checkshot calibration using Equation (16) with $\delta = -0.028$, arriving at the black curve which aligns with the checkshot values.

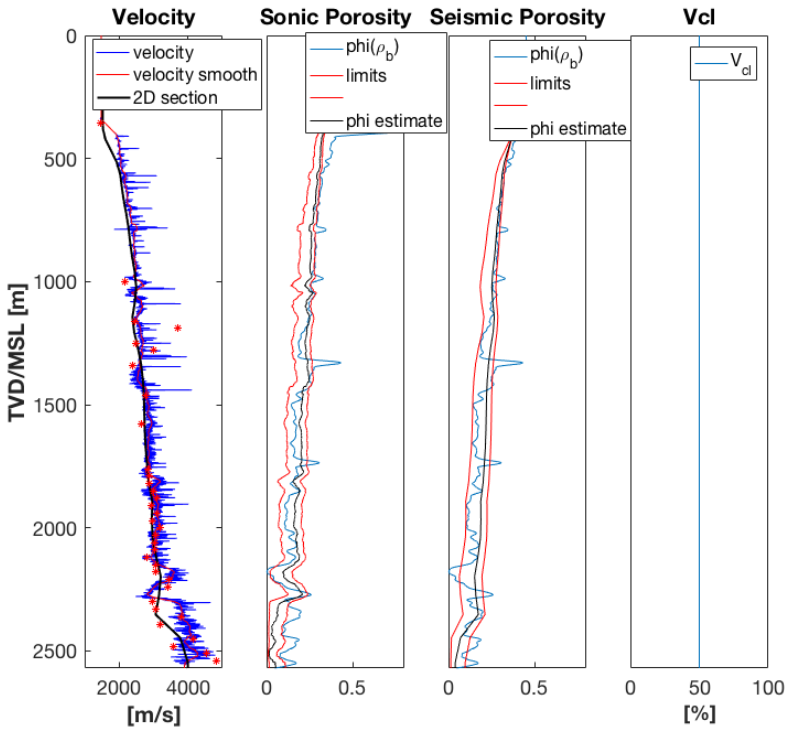

Figure 40: Left: The black curve is V_p-velocity extracted from 2D NMO interval velocity section in Figure (33) at well location. The blue curve is V_p-velocity from sonic-log. Middle: Estimated upper and lower porosity bounds along with estimated porosity, estimated from black curve in left plot. Right: Estimated upper and lower porosity bounds along with expected porosity, estimated from sonic-log curve in left plot. In both cases plotted with blue curve, porosity from density-log for comparison. Both estimations based on constant $V_{cl} = 50\%$. The red stars marked in the velocity plot are inverval velocity values calculated from the checkshot traveltime and depth values in Figure (34).

6.3.4 2D Porosity Profiles

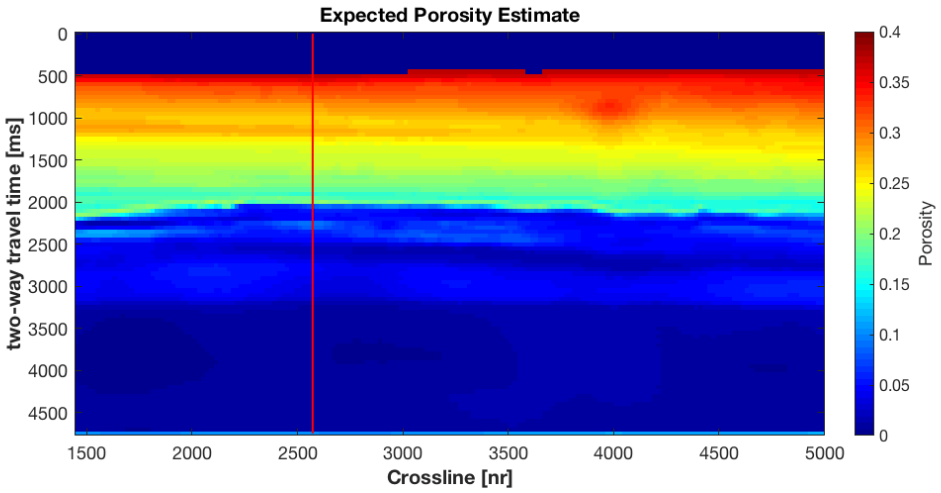

Figure 41: Estimated porosity porosity calculated for the entire 2D-section in Figure (33). This corresponds to the estimated porosity in Figure (35). Estimations based on constant V_{cl}=50%.

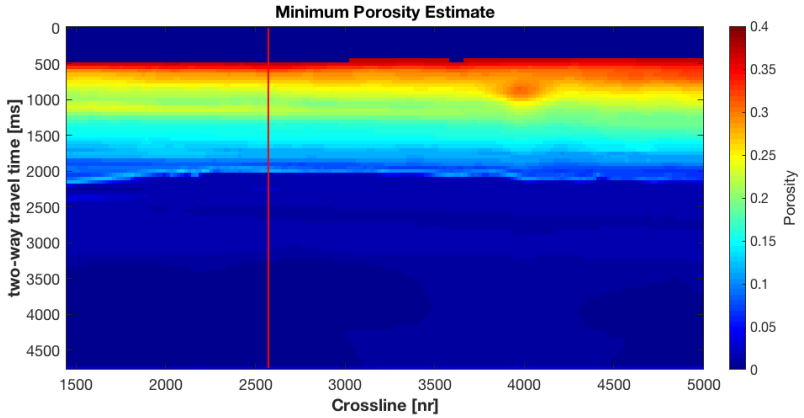

Figure 42: Lower porosity bound calculated for the entire 2D-section in Figure (33). This corresponds to the lower porosity bound in Figure (35). Estimations based on constant V_{cl}=50%.

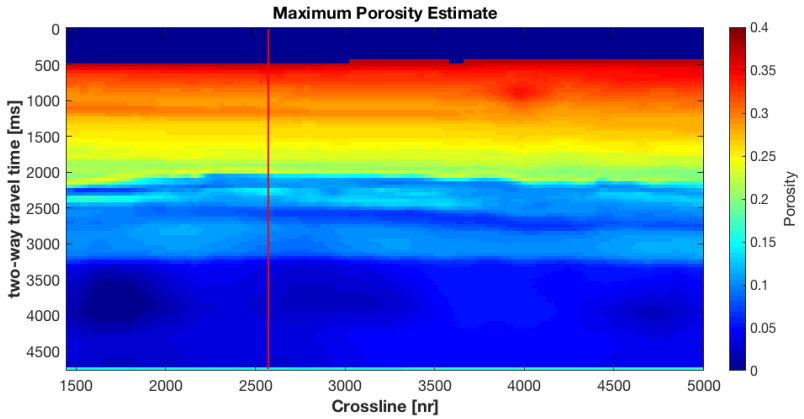

Figure 43: Upper porosity bound calculated for the entire 2D-section in Figure (33). This corresponds to the upper porosity bound in Figure (35). Estimations based on constant V_{cl}=50%.

7 Discussion

The principle aim of our study has been develop a simple modelling framework that estimates low frequent porosity trends in cases with sparse data. In other words we are interested in background porosity and not the exact porosity estimation in exact layers of interest.

The strength of our approach is the minimal need of p-wave velocity to perform estimations and the opportunity to improve estimations by including lithological information in the form of a clay content prediction.

We have applied our model to data sets gathered from three areas across the Norwegian Continental shelf; the Norwegian Sea , the North Sea and the Barents Sea. Our results clearly illustrates our models ability to estimate porosity trends in all three areas and our models ability to improve porosity estimations when improved lithological information is included.

The improvement of porosity estimations when using V_{cl} based on GR-log as lithological input, are illustrated in Figures (23, 27, 38). Estimated porosity values are closer to density derived porosity when lithological information is included, in all three cases. As well as improving porosity estimations, the improved lithological information gives us a increased sense of uncertainty in our porosity estimation by looking at the variation of the width of our porosity bounds.

Results derived from wireline velocity data indicate a tendency in our model to overestimate porosity when compared to density derived porosity. Overestimation of porosity may arise when clay content is under-predicted. As mentioned in Section (4.2) and illustrated in Figure (12), lower clay content will increase the porosity estimate. Our choice to use Hill-average in order to estimate porosity may also cause overestimations which I will discuss in relation to the Hashin-Strikman bounds.

If clay content is over-predicted we get the opposite effect; an underestimation of porosity. We believe this to be the case for the estimations performed on Snøhvit in Figure (35), where estimated porosity and its bounds indicate a slightly lower porosity trend for shallow depths than that indicated in the density-porosity. This may be caused by a constant clay content of $V_{cl} = 50\%$ being an over-prediction.

A decrease in clay content will result higher porosity estimations and wider bounds. Wider bounds indicate a higher degree of ambiguity in our estimation, i.e. a wider range of porosities that could produce the given velocity value. This is illustrated when estimating porosity for the Snøhvit well in Figure (37). With a V_{cl} estimate based on GR-log we arrive at much wider porosity bounds. This shows an innate property of our model whereby lower clay content increases the uncertainty of our porosity estimation and

widens the bounds of possible porosities.

It is important to take notice that and under/over -prediction of clay content may arise from a wrongful choice of GR_{max}/GR_{min}-values when estimating V_{cl} based on GR-log, as illustrated at the end of Section (4.2).

When considering the uncertainties in our porosity estimation it is critical to consider the uncertainties in our velocity data as it is the basis of our estimation. In seismic data the pressure waves are not propagating in vertical direction and are thus much more affected by potential positive anisotropy causing the velocities to appear higher as velocity increase when propagating in non-vertical directions. Keep in mind that seismically derived velocities is often derived to produce seismic images rather than the be used to estimate rock physical properties [Dutta, 2002].

Uncertainties in our porosity estimations may also relate to the validity of our assumptions. As we assume a binary rock system consisting of sand and shale only, which we know not to be the exact case in reality, we expect this assumption to be broken in many of our estimations. This may explain some of the deviations from the density-porosity curve in our results. The same can be said of our assumption of a minimum quartz content of $V_{qz.ma} = 20\%$ which may not be the case for some lithologies. And as we mentioned before; an over prediction of clay content will lead to underestimated porosity and under-prediction of clay content to overestimation of porosity. Despite our certainty that at some depths in our estimations these assumptions are broken, we are able to capture low frequency porosity trends to a satisfying degree. This emphasizes the agility of our model.

Regarding the Hashin-Strikman bounds described in Section (2.1), the upper bound can be seen as a "cementation-bound" where the grains are completely cemented and the lower bound can bee seen as a "suspension-bound" where the grains would be suspended in brine. This naturally explains why the lower bound approaches water velocity for higher porosities. It is worth noting that experimental studies have shown that at high porosities recorded velocity values will lie closer to the suspension bounds and at low porosities the velocity values will lie closer to the cementation bound. This makes the Hill-average, which is composed of the arithmetic average of bounds for bulk modulus and bounds for shear modulus, an inaccurate estimation of porosity at high and low range porosities Other possibilities for porosity estimation within the estimated bounds should be subject to further investigation.

8 Conclusion

A new composite model to estimate porosity from velocity data is derived by modelling elastic properties of sand using Hashin-strikman bounds, modelling elastic properties of shale using Vernik and interpolating between the two models. We have proven its ability to capture low frequent porosity trends in both wireline sonic data and seismically derived velocity data when comparing to what we assume to be true velocity derived from the density-log.

By including improved lithological information in the form an a V_{cl} prediction based on GR-log, we were able to improve the accuracy of the estimated porosity and its bounds. By including lithological information we can also look at the width of the estimated porosity bounds as a measure of the uncertainty of our estimated porosity.

By limiting our model to only take velocity and clay content as input, we are able to use the same model and methodology for a wide range of data sources. This allows our model to be used in both an exploration and a production setting.

9 Aknowledgments

I would like to extend my gratitue to my advisor Kenneth Duffaut for his continued guidance and commitment to this project. Our collabaration and idea sparring has been both educating and motivating.

I would also like to thank Børge Arntsen for providing us with velocity data derived from Full Waveform Inversion. The data and his work are detailed in Raknes et al. [2015].

Finally I would like to thank the Norwegian Petroleum Directory (NPD) and Statoil for their contribution of data and corresponding infromation.

References

R. Bachrach. Joint estimation of porosity and saturation using stochastic rock-physics modeling. *Geophysics*, 71(5):O53–O63, 2006.

J. G. Berryman, P. A. Berge, and B. P. Bonner. Estimating rock porosity and fluid saturation using only seismic velocities. *Geophysics*, 67(2):391–404, 2002.

M. A. Biot. Theory of propagation of elastic waves in a fluid-saturated porous solid. i. low-frequency range. *The Journal of the acoustical Society of america*, 28(2):168–178, 1956.

C. H. Dix. Seismic velocities from surface measurements. *Geophysics*, 20(1): 68–86, 1955.

P. M. Doyen. Porosity from seismic data: A geostatistical approach. *Geophysics*, 53(10):1263–1275, 1988.

N. Dutta. Geopressure prediction using seismic data: Current status and the road ahead. *Geophysics*, 67(6):2012–2041, 2002.

J. Dvorkin and A. Nur. Elasticity of high-porosity sandstones: Theory for two north sea data sets. *Geophysics*, 61(5):1363–1370, 1996.

J. Gassman and D. Smit. Some aspects of elastic wave propagation in uid saturated porous solids. *Geophysics*, 16:673–685, 1951.

J. Geertsma and D. Smit. Some aspects of elastic wave propagation in fluid-saturated porous solids. *Geophysics*, 26(2):169–181, 1961.

D.-h. Han, A. Nur, and D. Morgan. Effects of porosity and clay content on wave velocities in sandstones. *Geophysics*, 51(11):2093–2107, 1986.

Z. Hashin and S. Shtrikman. A variational approach to the theory of the elastic behaviour of multiphase materials. *Journal of the Mechanics and Physics of Solids*, 11(2):127–140, 1963.

R. Hill. The elastic behaviour of a crystalline aggregate. *Proceedings of the Physical Society. Section A*, 65(5):349, 1952.

R. G. Keys and S. Xu. An approximation for the xu-white velocity model. *Geophysics*, 67(5):1406–1414, 2002.

B. Kowallis, L. Jones, and H. Wang. Velocity-porosity-clay content systematics of poorly consolidated sandstones. *Journal of Geophysical Research: Solid Earth*, 89(B12):10355–10364, 1984.

G. T. Kuster and M. N. Toksöz. Velocity and attenuation of seismic waves in two-phase media: Part i. theoretical formulations. *Geophysics*, 39(5): 587–606, 1974.

G. Mavko, T. Mukerji, and J. Dvorkin. *The rock physics handbook: Tools for seismic analysis of porous media*. Cambridge university press, 2009.

H. W. Porten. Petrography, diagenesis and reservoir quality of the triassic fruholmen, snadd and kobbe formations, southern barents sea. Master's thesis, Norges teknisk-naturvitenskapelige universitet, 2012.

E. B. Raknes, B. Arntsen, and W. Weibull. Three-dimensional elastic full waveform inversion using seismic data from the sleipner area. *Geophysical Journal International*, 202(3):1877–1894, 2015.

L. Raymer, E. Hunt, J. S. Gardner, et al. An improved sonic transit time-to-porosity transform. In *SPWLA 21st annual logging symposium*. Society of Petrophysicists and Well-Log Analysts, 1980.

A. Reuss. Berechnung der fließgrenze von mischkristallen auf grund der plastizitätsbedingung für einkristalle. *ZAMM-Journal of Applied Mathematics and Mechanics/Zeitschrift für Angewandte Mathematik und Mechanik*, 9 (1):49–58, 1929.

M. Rider and M. Kennedy. The geological interpretation of well logs: Rider-french consulting, 2011.

C. Tosaya and A. Nur. Effects of diagenesis and clays on compressional velocities in rocks. *Geophysical Research Letters*, 9(1):5–8, 1982.

L. Vernik and M. Kachanov. Modeling elastic properties of siliciclastic rocks. *Geophysics*, 75(6):E171–E182, 2010.

L. Vernik and A. Nur. Petrophysical classification of siliciclastics for lithology and porosity prediction from seismic velocities (1). *AAPG Bulletin*, 76(9): 1295–1309, 1992.

W. Voigt. Ueber die beziehung zwischen den beiden elasticitätsconstanten isotroper körper. *Annalen der Physik*, 274(12):573–587, 1889.

M. R. J. Wyllie, A. R. Gregory, and L. W. Gardner. Elastic wave velocities in heterogeneous and porous media. *Geophysics*, 21(1):41–70, 1956.